Coupled multi-physics simulations of the Molten Salt Fast Reactor using coarse-mesh thermal-hydraulics and spatial neutronics

Master thesis by
Eirik Eide Pettersen

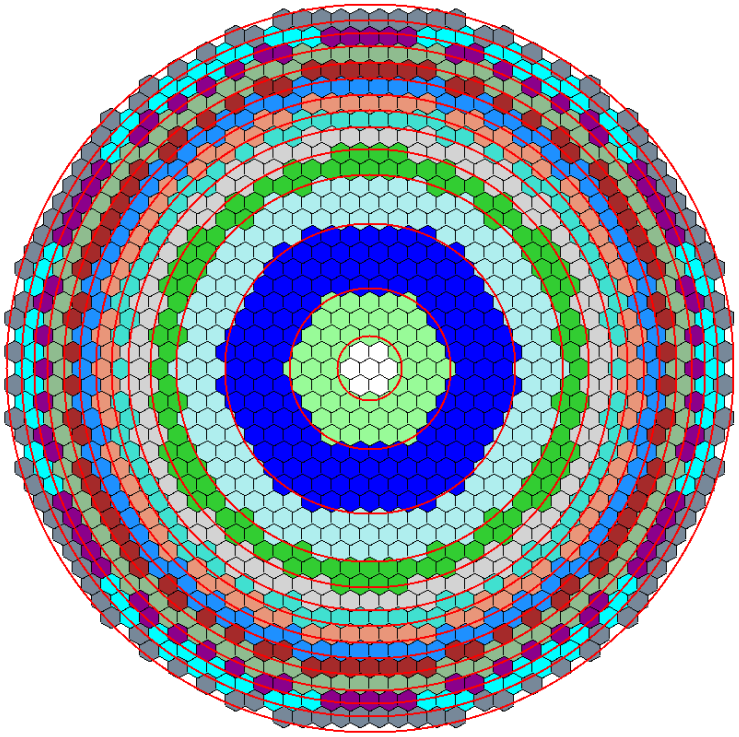

Supervised by:
Konstantin Mikityuk
@
Paul Scherrer Institut
Villigen, Switzerland

Université Paris-Saclay
September 2016

Abstract

The Molten Salt Fast Reactor (MSFR) perfectly embodies the tantalising prospects of next-generation nuclear power reactors by offering considerable improvements in areas of sustainability, safety, and economics, while avoiding greenhouse gas emissions. However, much research is needed to mature the conceptual design, not least in the field of computational physics. As with all liquid-fuelled molten salt reactors (MSRs), the MSFR is characterised by a particularly strong coupling between neutronics and thermal-hydraulics induced by combining the fuel and coolant into the same liquid. Investigations into the dynamic behaviour of MSRs thus require the use of coupled multi-physics codes. A number of such tools have emerged in recent years, most based on computational fluid dynamics (CFD).

In this thesis work, an alternative approach is taken with the use of a coupled tool consisting of the coarse-mesh, thermal-hydraulics system code TRACE and the three-dimensional neutron diffusion solver PARCS. This tool offers a number of advantages compared to CFD-based approaches, such as low computational requirements, established numerical solution and coupling methodologies, native two-phase fluid capabilities, and simplicity in modelling complex plant components across primary, intermediate, and turbine circuits. Conversely, the coarse-mesh and simplified equations solution strategy employed by TRACE-PARCS requires compromising the accuracy of the calculations, and suffers from limitations in problem geometry modelling. The overarching goal of this work is to assess the ability of the coupled TRACE-PARCS code to accurately compute dynamic behaviour of the MSFR. In doing so, many characteristic phenomena of molten salt reactors have been investigated. A secondary aim is to illustrate and explain these distinguishing and unconventional features.

Presented simulations of the MSFR have been performed in a simplified, axially-symmetric benchmark model implemented separately in both TRACE and PARCS, as well as in the Monte Carlo code Serpent which is used for cross section generation. Neutronic and thermal-hydraulic steady-state behaviour has been characterised and compared with alternative solvers. Following a calibration procedure, satisfactory agreement is found between steady-state solutions produced by TRACE and a higher-accuracy solver based on CFD. Similarly, the neutronic solution calculated by PARCS correlates well with Serpent after calibrating the boundary conditions. The coupled TRACE-PARCS code generally reproduces the dynamic behaviour of the MSFR as predicted by other multi-physics tools. Considerable discrepancies are present, but most are explained by differences in modelling choices, and those that remain are likely caused by dissimilarities in the underlying methods. Although TRACE-PARCS simulations could be run on a single processor, computational times were prohibitively long. Clear potentials for accelerating the computational procedure have been identified.

The presented work paves the way for further investigation of the MSFR, and allows for straightforward extension to full plant modelling and asymmetric transient investigation. Composite codes employing a CFD solver for core calculations coupled with TRACE for out-of-core components represent another promising direction in which to progress.

Contents

1 Introduction **5**

1.1 Background and motivation 5

1.2 Objectives and outline 7

2 Molten salt reactors **8**

2.1 History 8

2.2 Features 9

2.3 The Molten Salt Fast Reactor 10

2.3.1 Salts specification 12

2.3.2 Benchmark specification 13

3 Computational tools **15**

3.1 TRACE 15

3.1.1 Principal equations 15

3.1.2 Primary circuit model 17

3.1.3 Heat exchanger and pump models 18

3.2 Serpent 19

3.3 PARCS 20

3.4 Coupling methodology 21

4 Results **23**

4.1 Steady-state behaviour 23

4.1.1 Neutronics 24

4.1.2 Blanket behaviour 27

4.1.3 Thermal-hydraulics 28

4.2 Transient behaviour 34

4.2.1 Unprotected loss of heat sink 35

4.2.2 Unprotected pump over-speed 37
4.2.3 Unprotected over-cooling 38
4.2.4 Unprotected loss of flow 40

5 Conclusions and outlook **43**

References **44**

Appendices **50**

A Coupled code initialisation **50**

Acknowledgements **52**

1 Introduction

1.1 Background and motivation

Modern societies currently have but a few ways of generating reliable, non-intermittent base load power. These are, in no particular order: Hydro power, fossil fuels, biomass, and nuclear energy. In light of ever-increasing concerns over the heating of the atmosphere as a result of greenhouse gas emissions, sources that have negligible CO_2 footprints represent essentials measures for combating global warming. From an environmental point of view, these observations lead to a preference for hydro and nuclear power[1]. Since the potential for hydro power depends very much on local geographical conditions, conditions that many countries do not fulfil, one could argue that nuclear power should find wide utilisation around the world.

In reality, this is only partly true. Nuclear power currently provides about 5 % of the global energy production [IEA, 2015a], a figure which is projected to stay relatively constant up until 2040 [IEA, 2015b]. In comparison, these same projections foresee the contribution of coal to be around 30 % in 2040. This apparent apprehension towards a large-scale shift away from fossil fuels and to nuclear power stems from a number of factors, including deep-rooted concerns regarding radioactive waste treatment, safety, nuclear weapons proliferation, and ability to compete economically with other sources of energy. For all of these reasons, a negative public opinion of nuclear power has formed in many developed countries and created a challenging political scenery for advocating its climatic benefits.

The Molten Salt Fast Reactor (MSFR) is one attempt at overcoming the difficulties related to conventional nuclear power plants. As one of six advanced reactor designs selected by the Generation IV International Forum (GIF) for further research and development, it aims at offering significant improvements "in the four broad areas of sustainability, economics, safety and reliability, and proliferation resistance and physical protection." [GIF, 2002] Currently, these research efforts are being coordinated and pursued within the SAMOFAR project (Safety Assessment Of the Molten Salt Fast Reactor) consisting of a consortium of mainly European research institutions and industrial partners, including the Paul Scherrer Institut (PSI), as a part of the Horizon 2020 Euratom research programme. With a time frame spanning four years, the consortium seeks to develop and improve the main achievements of the preceding EVOL project (Evaluation and Viability Of Liquid fuel fast reactor system), and thereby further progress the MSFR concept towards industrial realisation.

To achieve the goals put forth by the GIF, molten salt reactors (MSRs) attempt to simplify the reactor core by using not only liquid coolant, but also liquid fuel.[2] Thus, fissile material is dissolved in the molten salt coolant and circulated in a loop-type primary circuit. This leads to immediate advantages over conventional nuclear reactors, some of which include near-atmospheric primary

[1] Contrary to popular belief, although biomass is a renewable energy source, recent research has shown that it is not necessarily beneficial for the environment over time scales that are relevant when considering global warming [Cherubini et al., 2011; Johnson, 2009].

[2] Molten salt-cooled reactors with solid fuel are generally also referred to as MSRs. However, in this thesis, MSRs are taken to be reactors with liquid fuel that also serves as coolant.

pressures, high outlet temperatures compatible with process heat applications, reduced fuel preprocessing, and the ability to continuously remove fission products and add fissionable and/or fertile material. As a result of continuous reprocessing, MSRs enjoy comparatively low excess reactivity, little decay heat, high burn-up, reduced waste production, and high capacity factors. Moreover, the reduction of absorbing core structures combined with the fast spectrum of the MSFR ensures a good neutron economy that allows for a wide range of fuel options as well as breeding capabilities further enhanced by the use of molten salt breeding blankets whose state as a liquid lends itself to reprocessing.

Despite numerous benefits, considerable challenges lie in the way of a commercial adoption of MSRs. These include, but are not limited to, identifying structural materials compatible with the corrosive, high-temperature, high-flux environment of the primary circuit, performing maintenance in the vicinity of the strongly irradiating fuel salt, engineering heater systems to avoid salt freezing in delicate components and melt frozen salt elsewhere, and proliferation concerns related to breeding blankets that can be used to produce high-quality fissile material. Furthermore, the characteristics of MSRs introduce computational challenges in accurately predicting dynamic behaviour. The aim of this work has been to address one of these, namely the inherent interdependence between different branches of reactor physics. Owing to the combining of the coolant and fuel in the same liquid, a particularly strong coupling is introduced between fields that traditionally have been more separated by fuel encapsulation. This is manifested by a strong temperature feedback and unconventional delayed neutron precursor (DNP) drift, among other things. As a consequence, tools that couple neutronics and thermal hydraulics are essential for correctly computing time-dependent phenomena in MSRs.

A number of such tools have emerged in recent years [Fiorina, 2013; Zanetti, 2016; Brovchenko, 2013; van der Linden, 2012; Li et al., 2014; Aufiero et al., 2014]. In common for most of these is their reliance on computational fluid dynamics (CFD) to solve the thermal-hydraulic problem, allowing for detailed modelling of turbulent effects on fine geometrical meshes within large, open salt volumes such as the MSFR core. The downside with a CFD-based approach is the computational efforts required, oftentimes demanding parallel execution on sizeable computer clusters to obtain adequately low run times. Since such computing capabilities have yet to reach widespread availability, much verification and validation work remain before CFD codes can be extensively adopted in the heavily regulated field of nuclear power. Moreover, circuit-scale CFD analyses require modelling of system components such as heat exchangers, primary and secondary pumps, secondary piping, steam generators, etc., which is not straightforward and often treated in a simplified manner. An alternative approach to CFD is to solve a simplified set of equations on a much coarser mesh, thus sacrificing accuracy for dramatically reduced computational requirements. Such tools, called system codes, are currently being applied to conventional LWR power plants in order to advise design decisions, study whole plant behaviour, and generate boundary conditions for higher-accuracy methods. Thus, they natively support both single- and two-phase fluid problems, and possess a high level of confidence on account of prolonged and extensive validation efforts. This confidence typically extends to a number of built-in component models that are easily tuned to the specific problem parameters, thereby simplifying the modelling process.

One tool that makes use of such accelerated solution strategy is the coupled TRACE-PARCS code package. In this, the best-estimate, NRC-developed thermal-hydraulics system code TRACE (TRAC/RELAP Advanced Computational Engine) [NRC, 2007] calculates temperature, pressure, and velocity fields on coarse meshes while ignoring turbulent effects. As a result, the code routinely solves plant-scale thermal-hydraulic problems on a single processor within a manageable time frame. Not long ago, TRACE was extended with molten salt modelling and DNP transport capabilities [Zanetti et al., 2015], allowing it to calculate distributions of DNPs in liquid-fuelled reactors. In [Zanetti et al., 2015], it was also fitted with a point-kinetics solution routine that produced results in good agreement with higher-accuracy codes. A natural continuation from a point-kinetics approach is to consider the three-dimensional neutronics problem in order to account for spatial

variations in the thermal-hydraulic solution. Thus, in the coupled system, PARCS (Purdue Advanced Reactor Core Simulator) [Downar et al., 2009], a deterministic, three-dimensional neutron kinetics solver also belonging under the auspices of the NRC, receives the DNP and temperature fields, and calculates the spatial power distribution, which is then returned to TRACE. Although originally developed for use with thermal LWRs, PARCS has been adopted for fast reactor analysis at PSI [Mikityuk et al., 2005]. The macroscopic cross sections employed by PARCS in this process can be supplied by any compatible cross section generator. For this work, the Monte Carlo code Serpent [Leppänen, 2013] was chosen. This particular combination of TRACE-PARCS in conjunction with Serpent represents the latest developments of the FAST code system [Mikityuk et al., 2005] developed and curated by PSI, and has recently been successfully applied to the Molten Salt Reactor Experiment [Kim, 2015].

1.2 Objectives and outline

This thesis reports the application of the coupled TRACE-PARCS code to the MSFR, which represents the continuation of the work presented in [Kim, 2015] and [Zanetti, 2016]. Three areas of advancements from these previous works can be readily distinguished. First, and related to [Kim, 2015], the coupled TRACE-PARCS code is herein applied to a larger and more complex reactor (in terms of flow field) than the MSRE. Second, the fixed-shape, point-kinetics neutronics solution utilised in [Zanetti et al., 2015] is replaced with the spatial power solution calculated by PARCS. Third, improvements aimed at modelling the MSFR heat exchangers in a more realistic manner have been implemented.

Despite extensive efforts in verification and validation of the codes used, both as standalone codes and coupled together, their intended usage has always been existing light water reactors. Consequently, legitimate concerns regarding the applicability of the coupled system to the MSFR exist. An assessment of its ability to recreate characteristic dynamic behaviour of the MSFR is therefore conducted, and represents the overarching objective of this work. This assessment is envisaged to pave the way for further and more extensive analysis of the MSFR. For performing transient simulations, steady-state results of the MSFR from the separate tools must first be obtained. A second objective of this thesis is to illustrate and explain some of the distinguishing features of molten salt reactors based on both the steady-state and dynamic calculations that have been performed.

The structure of the thesis is as follows. In chapter 2, the history of MSRs is briefly recalled and their main defining characteristics and associated consequences are listed. Particular focus is given to the MSFR, and the specifications of the modelled benchmark are presented. Chapter 3 covers the three different computational tools and models implemented in each of them. In an attempt to avoid the pitfalls of a black box understanding and to identify model limitations at an early stage, governing equations and working principles are stated and discussed. The synthesis procedure of the three separate codes into the coupled multi-physics tool is then presented. Both stationary and transient results from standalone and coupled calculations are given in chapter 4. Additionally, comparisons are made with available computational data from other works accompanied by brief analyses and discussions. In the last chapter, an attempt is given at summarising the work and a conclusion is offered together with an outlook for future work on the subject. Finally, the single appendix details the particularities of the procedure established for initialising the transient simulations, and is included for replication purposes.

2 Molten salt reactors

With the renewed research focus stimulated by the selection into the GIF in 2002, molten salt reactors have of late enjoyed a revival of interest not only contained to academia. The emergence of a handful of start-up companies with the explicit purpose of commercialising MSR technology exemplifies this notion. With that being said, the MSR concept already possesses a surprisingly long and eventful backstory, which is instrumental in understanding the enthusiasm it receives today. In this chapter, a brief summary of this history is offered, followed by some of the attractive features that warrants this persisting interest. Thereafter, the contemporary MSFR concept is presented together with the particularities of the benchmark specification followed in this thesis work.

2.1 History

As stated, the idea of a nuclear reactor circulating a molten salt mixture that combines coolant and fuel is no modern conception. The first mentions of such a design dates back to the late 1940's, around the time of the inception of nuclear power production. At the forefront of MSR development in this period were two experimental efforts led by and operated at Oak Ridge National Laboratories (ORNL) in the US, called the Aircraft Reactor Experiment (ARE) and the Molten Salt Reactor Experiment (MSRE). These projects remain the only experiments in which MSRs have been operated to this day.

The world's first MSR to be constructed, the ARE, reached criticality in November 1954. It was a 2.5 MW_{th} reactor fuelled by enriched uranium dissolved in a NaF-ZrF_4-UF_4 salt and moderated by blocks of beryllium oxide. With the stated purpose of propelling bomber air planes for sustained periods of flight, it represented an effort to improve America's range and response time during the restlessness of the Cold War. Thus, although the experiment reported successful operation, the maturation of intercontinental ballistic missiles soon made the concept obsolete and funding was discontinued.

Still convinced by the benefits of liquid-fuelled reactors, the next molten salt project started construction at ORNL in 1962, and three years later the MSRE first reached criticality. Bigger than its predecessor, it was designed to reach 10 MW_{th} by fissioning uranium in the form of LiF-BeF_2-ZrF_4-UF_4 salt circulated through channels in a graphite-moderated core. Its purpose also differed markedly from the ARE, as the MSRE was built to demonstrate the commercial potential of a simple yet safe molten salt-based reactor design. Over the next four years, the MSRE performed favourably and in 1968 became the first reactor to sustain a chain reaction using ^{233}U [Haubenreich and Engel, 1970]. Nevertheless, despite convincing results, further MSR development was hindered by a lack of funding. At a time where fissile resources were thought to be scarce, the US chose to prioritise the liquid metal fast breeder concept [MacPherson, 1985]. As a result, the follow-up project to the MSRE, the 1000 MW_e Molten Salt Breeder Reactor (MSBR), never left the drawing board.

2.2 Features

The distinguishing characteristic of MSRs is the combination of coolant and fuel into the same liquid, a particularity that carries with it a number of features, some of which are unique to MSRs. These features can broadly be split into categories for safety and economics.

In terms of safety, one of the simplest yet strongest arguments in favour of MSRs is their inability to experience core meltdown in a similar way as conventional solid-fuelled reactors. Instead, provisions must be made to avoid fuel boiling scenarios that might exert excessive pressures on enclosing components and volatilise radionuclides. However, as most fuel salts under consideration have a fairly high specific heat capacity (comparable to water [Samuel, 2009]) and large margin-to-boiling at nominal reactor temperatures, comparatively much time (compared to water) is available during loss of cooling accidents.[3] Furthermore, if all active cooling systems were to be disabled, liquid fuels can still be cooled by several passive means, most notably natural circulation and freeze plugs that melt and drain the core to a purpose-built tank. Based on these considerations, salt boiling has been neglected in this work.

An added benefit of the large margin-to-boiling is that it reduces the need for pressurising the primary circuit and thus allows MSRs to operate at near-atmospheric pressures. Since molten salts also are chemically inert and will not undergo exothermic chemical reactions, concerns regarding the containment of radioactive materials are greatly alleviated.[4] The same is true when assessing radiological impacts of severe accidents in which fuel salt reaches the environment, for two reasons. First, fluoride-based salts have excellent fission product and actinide retention abilities at high temperatures that counteracts rapid dispersion [Forsberg et al., 2003; Beneš and Konigs, 2012b]. Second, volatile fission products that are not soluble in the fuel such as noble gases, can be removed from the primary circuit and safely disposed off in a continuous manner. This principle was successfully demonstrated with the MSRE where a spray system was used to effectively remove xenon from the primary salt inventory [Kedl, 1972; Rosenthal, 2009]. As a result, both the source term and decay heat is decreased, while xenon reactivity effects are made insignificant. Moreover, with volatile neutron poisons such as xenon continuously removed and the ability to compensate for fuel depletion through on-line refuelling and fissile breeding, very little excess reactivity is required at any time. In the specific case of fast reactors, this is even truer as the influence from the remaining fission products is suppressed by the fast spectrum. The total reactivity worth of the control system can therefore be designed low (a "weak" system), so as to limit the potential for reactivity-induced accidents originating from operator error or system malfunction.

Lastly, liquid-fuelled reactors also generally possess very favourable temperature feedback coefficients. In addition to Doppler effects, expansion of the fuel salt with increasing temperature reduces the density of fissile material and, subsequently, also the reactivity. As an example, for the MSRE the combined effect was measured to (-4.9 $\pm$ 2.3) pcm/K [Haubenreich and Engel, 1970].

Several features of MSRs can contribute to improving their economical aspects. For instance, with comparatively large power densities unrestricted by fuel centre line temperatures, reduced material and construction expenditures can be expected and further augmented by the avoidance of strict pressure requirements. Furthermore, production costs related to fuel pin and fuel assembly fabrication are avoided, while the ability to perform on-line refuelling and fission product removal limits downtime to maintenance outages and consequently leads to high capacity factors as well as efficient fuel usage. This, in turn, means that MSRs produce less long-lived radioactive waste. The high outlet temperatures of MSRs can also prove beneficial by enabling plants to operate at high

[3] Obviously, the ordinary expression "loss of coolant accident" is not entirely appropriate for MSRs and would represent a far more severe accident.

[4] One notable exception to this is tritium that is produced in copious amounts when salts containing lithium are exposed to neutron irradiation and readily permeates most radiological barriers. This concern was noted by ORNL engineers in their MSRE reports, and a solution has since been proposed [MacPherson, 1985].

thermal efficiencies, as well as granting entry to high-temperature process heat markets traditionally served by non-nuclear technologies. Among these are hydrogen and ammonia production, and fossil fuel extraction and refinement processes [Sabharwall et al., 2011].

Lastly, MSRs offer great flexibility in terms of nuclear fuel cycle and mode of operation, and can be utilised as ordinary burners, iso-breeders, or breeders. In fact, the fuel reprocessing process is simplified for liquid-fuelled compared to solid-fuelled breeders, in which dissolution of the fuel into a liquid feature as an intermediate step. Through the use of separate salt compartments circulating fertile material in relatively high flux regions, i.e., breeding blankets, the process can be further simplified. Combined with good prospects for utilising thorium, a fuel whose potential benefits are widely reported in literature [Sokolov et al., 2005; Penny, 2010; NEA, 2015; Kakodkar and Degweker, 2013], MSRs could represent a more sustainable nuclear fuel cycle that makes more efficient use of natural resources and produces less long-lived waste than the once-through fuel cycle that dominates the industry today.

There are also disadvantages associated with liquid-fuel molten salt designs. First, the transport of the fuel means that a lower fraction of DNPs resides within the core region at any time. Thus, the effective delayed neutron fraction, β_{eff}, is lowered compared to solid-fuelled reactors, reducing safety margins and complicating reactor control. Second, the relatively high melting temperature of the salt requires an intricate system of heaters that are able to heat parts of the salt-circulating circuits in order to avoid salt freezing or, alternatively, allow for salt thawing and melting. Third, materials that can withstand high temperatures, salt corrosion, and intense neutron irradiation are required for the core region. Fourth, the significant negative temperature coefficient demands careful temperature control of salt entering into the core as over-cooling has the potential to introduce considerable positive reactivity. Fifth, costly remote handling systems will be required for any manual labour that has to be conducted in the vicinity of the primary circuit, as well as generous shielding.

Other aspects related to the construction and operation of a molten salt reactor breeding uranium from thorium could also prove problematic. This includes serious concerns related to proliferation, as any thorium-fuelled two-fluid design that removes protactinium and lets it decay out-of-core will have to make security-related provisions for guarding what will eventually become high-quality ^{233}U. Moreover, although expected to be easier than reprocessing and extracting fissile material from solid fuel, significant research efforts remain in the development of a safe and efficient scheme for on-site handling and chemical treatment of the highly radioactive primary salt on a continuous basis [Mathers and Hesketh, 2013].

Besides technical challenges associated with MSRs, there are administrative hurdles. In particular, after more than half a century of a nuclear industry almost exclusively consisting of water-cooled reactor technologies, a certain rigidity has formed in nuclear regulations to adhere to traditional safety approaches meticulously developed and matured over decades for this particular technology. With the introduction of radically different designs such as liquid-fuelled reactors, new concepts in safety regulations are also required in order to update existing regulatory framework. To that purpose, some preliminary activities have started [NRC, 2012; Brovchenko, 2013; CNSC, 2015].

2.3 The Molten Salt Fast Reactor

Recent European interest in MSRs has seen a shift away from MSRE-inspired designs and towards a non-moderated concept [Mathieu et al., 2006; Merle-Lucotte et al., 2008], now known as the Molten Salt Fast Reactor. There are several reasons for this, one of which is the eventual deterioration of the core graphite under irradiation. For smaller reactors with a comparatively low expected life span (e.g. small modular reactors that are easily replaced, either partially or entirely), this does

not necessarily pose a great problem. However, for large, centralised power stations benefiting from economy-of-scale and operating for several decades, replacement of the graphite would become a very real possibility [Nagy et al., 2010]. Another reason to prioritise a fast spectrum reactor is that breeding benefits from less sterile captures in structures, fission products, and actinides, as well as an increased fission neutron yield from ^{233}U. The net effect is that iso-breeding can be accomplished at a much lower rate of salt reprocessing compared to graphite-moderated MSRs (as an example, reprocessing rates are predicted to be about two orders of magnitude smaller for the MSFR than the epithermal MSBR [Auger et al., 2008]). Lastly, a design without graphite has advantages in terms of temperature feedback coefficients that remain reassuringly negative at all temperatures. It has been found that this is not necessarily the case for the MSBR [Mathieu et al., 2006].

The MSFR is planned to be a 3 GW_{th}/1.5 GW_e fast-spectrum reactor optimised for simplicity and safety. Thus, the reactor core is designed with a minimum of internal structures, as illustrated in figure 2.1. Its main characteristics are summarised in table 2.1.

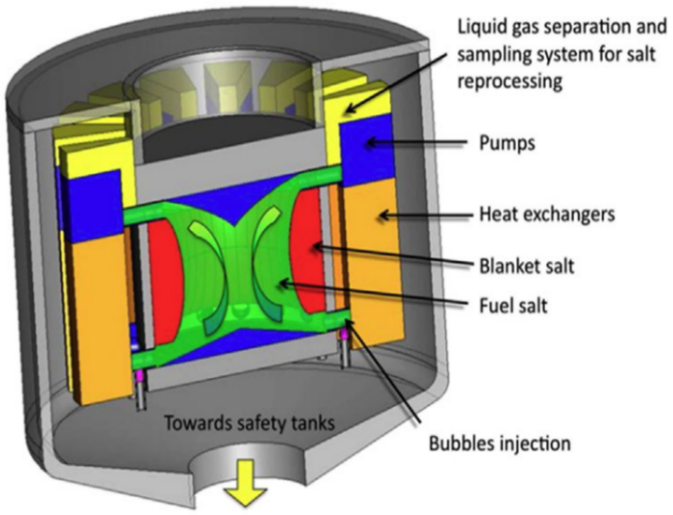

Figure 2.1: Conceptual design of the MSFR [Serp et al., 2014]. It should be noted that the design is not finalised, and experiences iterative improvements as more is learned about the concept.

Parameter	**Value**
Power	3 GW_{th} / 1.5 GW_e
Salt volume	18 m^3
Salt fraction in core	50 %
Number of circulation loops	16
Nominal flow rate	18500 kg/s $\approx$ 4.5 m^3/s
Nominal circulation time	4.0 s
Inlet / outlet temperature	973 K / 1073 K (700 °C / 800 °C)
Blanket volume	7.3 m^3

Table 2.1: Main properties of the MSFR benchmark specification.

For extracting the power generated in the MSFR, 16 independent circulation loops transfer the heat to an intermediate salt circuit which, in turn, is connected to a tertiary circuit that produces electricity or process heat. Each of these 16 primary loops consists of a fuel pump, heat exchanger, and associated piping and instrumentation. As a result, the failure of a single circulation loop will not reduce core cooling to the same extent had there only been a few pumps. Following a modular design philosophy, the circulation loops are to be constructed as separate compartments that are installed on the outside of the core. This ensures good accessibility and availability for maintenance,

as well as simple compartment replacement procedures. Surrounding the core in the radial direction are tanks in which a blanket salt with fertile material will be circulated for breeding purposes, while reflectors cover the top and bottom. Behind the breeding blankets, a layer of absorbing material is placed to minimise neutron irradiation of the pumps and heat exchangers. Located at the bottom of the reactor and penetrating the reflector are connections to the actively-cooled freeze plug that will melt and drain the core under severe accident conditions involving loss of power or overheating of the fuel salt. Also penetrating the reflector are connections to an expansion vessel situated above the core and used for maintaining a constant primary pressure.

Of particular interest with the current MSFR design is the complete lack of control or safety rods [Pioro, 2016]. Instead, the reactivity of the core is to be controlled by taking advantage of the negative Doppler and salt density coefficients, as well as the possibility of rapidly modifying the core geometry through drainage. As a result, reactivity can be controlled during nominal and accidental operating conditions. In the former, by varying the flow of salt passing through the core and the heat exchangers, the core temperature, and therefore reactivity, can be effectively controlled. Moreover, if excessive temperatures would have to be reached for lowering reactivity sufficiently, options for reducing fuel density by the introduction of gas bubbles also exist. During accidental conditions, subcriticality is achieved by transferring the fissile material to a subcritical geometry, i.e., the drain tanks.

Owing to the fast neutron spectrum, pictured in figure 4.1, the continuous reprocessing, and the reduction of internal structures that would otherwise absorb neutrons, the MSFR is able to run on a wide range of different fuels. This includes uranium-plutonium, uranium-thorium, and as a transmuter burning mixtures of fresh fuel and transuranic elements from used fuel in an effort to alleviate nuclear waste concerns [Fiorina et al., 2013]. The main intended purpose of the MSFR, however, is to function as a thorium breeder in a closed fuel cycle [Merle-Lucotte et al., 2011]. With a calculated maximum breeding ratio of about 1.1 [Fiorina, 2013], one MSFR is able to produce sufficient fissile material to sustain power production and generate an excess for starting up a new reactor within a relatively modest time frame. This allows for good deployment capabilities, which are further improved by the ability to ignite MSFRs using enriched uranium and/or plutonium stockpiles. In such closed fuel cycle, only thorium would have to be mined and supplemented to the reactor inventory, thus greatly reducing the pressure on natural resources from using ^{235}U as the fissile driver, as well as ensuring a fixed fuel cost undisturbed by fluctuations in electricity prices. At the other end of the fuel cycle, the back-end will benefit from a greatly diminished long-lived waste production.

2.3.1 Salts specification

At the current stage of development, only the fuel and blanket salts of the MSFR have been characterised. These are both LiF-AcF_4, where Ac represents an actinide, chiefly thorium or uranium for the thorium fuel cycle option. To minimise the salt melting temperature, the mole fractions of LiF and AcF_4 are set to 77.5 % and 22.5 %, respectively, which is the eutectic point. Sterile captures are kept low by using lithium enriched to 99.995 % in ^{7}Li. In order to further simplify the computational procedures, pure ^{7}Li is assumed in this work. For steady-state neutronic calculations of the MSFR at a uniform temperature, this assumption led to a 33 pcm increase in reactivity, which is tolerable. The thermal-hydraulic properties of the fuel and blanket salts are summarised in table 2.2, and were added to the TRACE source code during recent work performed at PSI [Zanetti et al., 2015]. It should be noted that in all simulations where temperatures entered outside of the stated validity ranges of the experimental basis, the expressions were extrapolated, with one exception. For the specific heat, the interval average $c_p = 1355$ J/kg/K was used.

For performing the computations presented herein, a decision was made to simulate an MSFR start-up core consisting solely of ^{232}Th and ^{233}U. The reactor was then made to be critical in

Serpent at a uniform core temperature of 1030 K, approximately corresponding to the average core temperature obtained from steady-state thermal-hydraulics calculations by TRACE. The resulting fuel salt composition is given in table 2.3 together with the blanket salt composition.

Property	**Symbol**	**Expression**	**Validity**
Melting temperature [K]	T_{melt}	841	1 bar
Boiling temperature [K]	T_{boil}	1874	1 bar
Density [kg m^{-3}]	ρ	$4094 - 0.882 \cdot (T - 1024)$	(893-1125) K
Dynamic viscosity [Pa s]	μ	$\rho \cdot 5.54 \cdot 10^{-8} \cdot \exp(3689/T)$	(898-1121) K
Thermal conductivity [W m^{-1} K^{-1}]	k	$0.928 + 8.397 \cdot 10^{-5} \cdot T$	(891-1020) K
Specific heat [J kg^{-1} K^{-1}]	c_p	$-1111 + 2.78 \cdot T$	(867-907) K
Saturation pressure [Pa]	p_{sat}	$10^{(11.902 - 12989/T)}$	(839-1473) K

Table 2.2: Experimentally-deduced properties of the LiF-AcF_4 (77.5 - 22.5 %-mole) fuel and blanket salt [Rouch et al., 2014]. The properties are assumed to vary negligibly with actinide composition.

	Isotope	**Mole fraction [%]**	**Total inventory [kg]**
Fuel salt	^{7}Li	29.0	4456
	^{19}F	62.6	26079
	^{233}U	1.0	4937
	^{232}Th	7.4	37871
Sum			73343
Blanket salt	^{7}Li	29.0	1814
	^{19}F	62.6	10616
	^{232}Th	8.4	17417
Sum			29847

Table 2.3: Isotopic compositions of the LiF-AcF_4 (77.5 - 22.5 %-mole) fuel and blanket salts.

For the MSFR intermediate salt, a number of alternatives are still under consideration. Among these is the 2:1 mixture of LiF and BeF_2, also known as FLiBe, which has been used in the intermediate circuit in this work. Its thermal-hydraulic properties are given in table 2.4.

2.3.2 Benchmark specification

In this thesis, a simplified benchmark geometry of the MSFR has been studied. There are several reasons for this choice. First, by choosing an established benchmark geometry, a number of previous studies on the same problem exists with which comparisons can be made [Fiorina, 2013; Zanetti, 2016; Brovchenko, 2013; van der Linden, 2012; Li et al., 2014]. Second, both TRACE and PARCS are unable to describe models with intricate geometrical complexities. In the former, the user is restricted to choosing between Cartesian or cylindrical geometries. In the latter, the problem geometry is modelled with fuel assemblies arranged in either a square or hexagonal lattice. Third, since the MSFR design is not yet finalised, subsequent design changes will more likely than not eventually render the most up-to-date design obsolete as well.

The simplified benchmark geometry describes the MSFR core as a cylinder of equal height and diameter, so as to both minimise neutron leakage and simplify modelling efforts. For the out-of-

core components, axial symmetry is assumed so that no individual circulation loops are explicitly described. As a result, the entire primary circuit can be modelled as a cylinder from which regions representing the blanket and absorber are cut out. The benchmark also does not characterise the pumps or heat exchangers, leaving great freedom in how to obtain the prescribed inlet temperature and mass flow rate. Figures 2.2a and 2.2b illustrate this benchmark geometry from the side and from the top, respectively.

Property	**Symbol**	**Expression**
Melting temperature [K]	T_{melt}	728
Density [kg m^{-3}]	ρ	$2146.3 - 0.4884 \cdot T$
Dynamic viscosity [Pa s]	μ	$1.81 \cdot 10^{-3} \cdot \exp(1912.2/T)$
Thermal conductivity [W m^{-1} K^{-1}]	k	1.1
Specific heat [J kg^{-1} K^{-1}]	c_p	2390
Saturation pressure [Pa]	p_{sat}	$10^{(11.914-13003/T)}$

Table 2.4: Properties of the LiF-BeF_2 (66.7 - 33.3 %-mole) intermediate salt [Beneš and Konigs, 2012a].

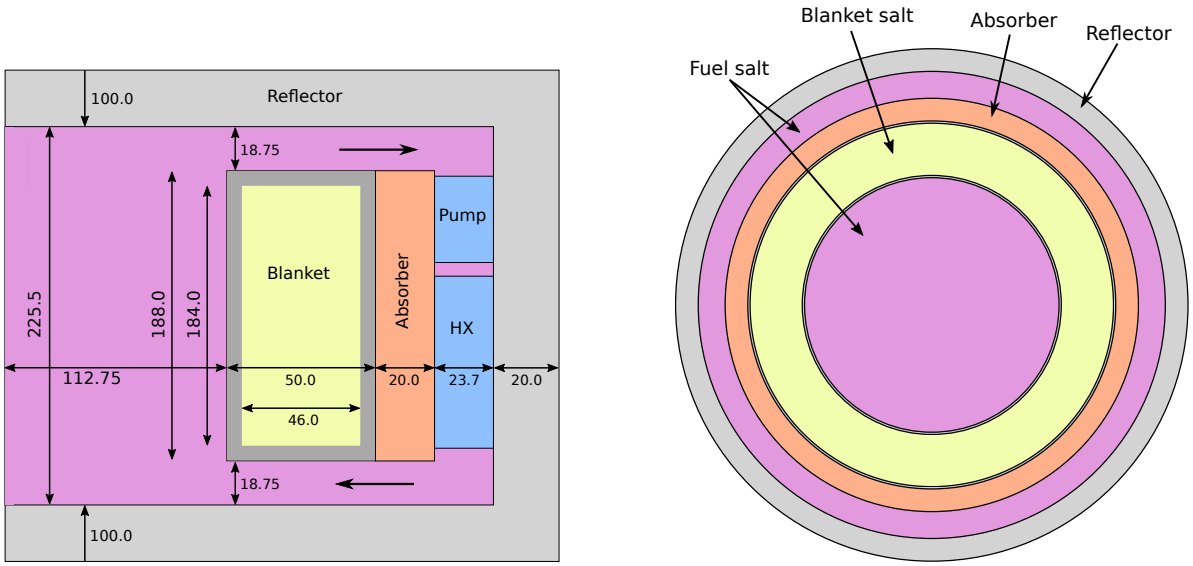

(a) Cross-sectional side view. Note that the drawing is not to scale.

(b) Cross-sectional top view.

Figure 2.2: Illustrations of the axially-symmetric MSFR benchmark geometry. All dimensions are in centimetres.

All structural materials, that is, the blanket salt tank and reflector materials, have been taken to be a nickel alloy with a density of 10 g/cm^3. The layer of absorbing material shielding the pumps and heat exchangers is boron carbide with a density of 2.52 g/cm^3, while the heat exchangers have been modelled consisting of Hastelloy-N. Table 2.5 lists the elemental compositions of these materials.

	Element	B	C	Al	Si	V	Cr	Mn	Fe	Ni	Mo	W
A.f. [%]	**Absorber**	80	20	-	-	-	-	-	-	-	-	-
	Structure	-	-	0.3	-	-	7.0	-	-	67.7	-	25.0
W.f. [%]	**HXs**	-	0.06	≤0.5	≤1	≤0.5	7	≤0.8	≤4	71	16	≤0.5

Table 2.5: Elemental composition of the various materials used in the modelling of the MSFR [Haynes International, 2015; Aufiero, 2014]. A.f. refers to atomic fraction, while w.f. denotes weight fraction.

3 Computational tools

Three distinct tools were used over the course of this project: The thermal-hydraulics system code TRACE developed by the NRC, the Monte Carlo neutronics code Serpent (v.2.1.26) under active development at the VTT Technical Research Centre of Finland, and the deterministic neutronics solver PARCS from Purdue University. In this chapter each of these codes will be briefly presented. Particular focus will be put on the underlying equations that are being solved in an attempt to understand the assumptions and simplifications that inevitably limit the accuracy of the solution produced. In addition to this, the particularities of the different implementations of the benchmark problem in each tool are described. Lastly, the methodology for combining these three separate tools into a single, coupled multi-physics solver is covered.

3.1 TRACE

The TRAC/RELAP Advanced Computational Engine is a thermal-hydraulics system code that solves the conservation of mass, momentum, and energy for two-phase flows subjected to internal and external heat transfer using finite volume numerical methods. It does so for 0D, 1D, and 3D geometries, and generally on fairly coarse computational meshes over which the problem variables are averaged. Integral quantities are then represented in mesh centre points, while those with directions are stated on the mesh boundary corresponding to the direction of the quantity. For instance, the velocity component in an arbitrarily defined x direction within a cell will be specified on the face of the cell whose normal vector points in the x direction. This is known as a staggered mesh [Patankar, 1980]. The thermal-hydraulic problem to be solved is formulated through the use of built-in components defined within TRACE. These include components representing one-dimensional pipes, pumps, and plenums, three-dimensional vessels, as well as solid heat structures and distributed power components. All components that carry fluid can then be subdivided into cells of arbitrary sizes. The specification of three-dimensional cells illustrate one restriction related to the usage of TRACE, as users can only choose between Cartesian or cylindrical geometries.

3.1.1 Principal equations

Within all flow-carrying components, the aforementioned equations are solved. The exact formulations are [NRC, 2007] (c.f. the nomenclature for description of symbols)

$$\frac{\partial \rho}{\partial t} + \nabla \cdot \rho \boldsymbol{u} = 0, \tag{3.1}$$

for the conservation of mass,

$$\frac{\partial (\rho \boldsymbol{u})}{\partial t} + \nabla \cdot (\rho \boldsymbol{u} \cdot \boldsymbol{u}) + \nabla p = \boldsymbol{f_w} + \rho \boldsymbol{g}, \tag{3.2}$$

for the conservation of momentum, and

$$\frac{\partial[\rho(e+u^2/2)]}{\partial t} + \nabla \cdot [\rho(e + \frac{p}{\rho} + u^2/2)] = q_w + q_f + \rho \boldsymbol{g} \cdot \boldsymbol{u} + \boldsymbol{f_w} \cdot \boldsymbol{u}, \tag{3.3}$$

for the conservation of energy. In these equations, Reynolds averaging is applied to each calculated quantity so as to ignore small temporal fluctuations and obtain time-averaged behaviour. Thus, calculated quantities are averaged both in space and time. TRACE also contains a similar set of equations describing the gas state of the fluid. However, since the margin-to-boiling for the molten salts in the MSFR is substantial, these equations as well as the terms describing interfacial exchange of mass, momentum, and energy are not resolved in the simulations presented herein. That being said, while molten salt boiling is out-of-scope at the current stage of development of the MSFR design, it is clearly a topic that will demand attention as the concept matures. Moreover, the primary salt will contain bubbles of fission product gases and tritium, among other things, that will require salt-gas flow equations to resolve.

Also neglected in the energy conservation equation above is the term describing heat conduction within the fluid. In TRACE, the inclusion of this term is activated or deactivated through user input. Since the salts used in the MSFR typically have relatively large Prandtl numbers [Fiorina, 2013] so that convective heat transfer dominates, the option has been deactivated.

The wall friction force term, f_w, deserves scrutiny. It describes frictional forces on pipe flow and is defined as

$$\boldsymbol{f_w} = C_w \boldsymbol{u}|\boldsymbol{u}|, \tag{3.4}$$

where the wall drag coefficient is given as

$$C_w = k_w \frac{2\rho}{D_h}, \tag{3.5}$$

and $k_w = k_w(Re, D_h, \delta)$ is the Churchill correlation friction factor [NRC, 2007]. Not included in this friction term, nor anywhere else in the above formulations, are viscous shear stresses or turbulence effects such as those included in the k-ϵ turbulence model or similar models. These terms are neglected in TRACE. As a consequence, the code can not be expected to accurately recreate flow behaviour that is significantly affected by turbulence, including large, open flow regions that exhibit recirculation zones. Note that this point is of particular importance for the results presented in the below, as turbulence effects are very much present in the MSFR core where the Reynolds number may reach 10^6 [van der Linden, 2012].

An additional assumption is made in TRACE for calculating the convection term of the momentum conservation equation, $\nabla \cdot (\rho \boldsymbol{u} \cdot \boldsymbol{u})$, in multi-dimensional geometries. When cell surface velocities on the staggered mesh are used to estimate the momentum flux at cell centres, momentum convection is assumed to only be performed by the velocity component in the same direction as the momentum flux component being calculated. In other words, cross-derivative terms of the divergence operator are ignored. The severity of this approximation varies with cell size, as well as the amount of flow mixing in the core.

In this work, the entire primary circuit of the MSFR was modelled within one three-dimensional, axially symmetric *vessel* component using the cylindrical geometry option. When using *vessel* components, it is possible to define the hydraulic diameter for each cell in both radial and axial directions. By taking advantage of the functional dependence of the friction factor defined in equation 3.5 (it can be shown to decrease uniformly with increasing D_h), artificial drag can be

introduced away from physical walls in order to alleviate the lack of viscous shear stresses within the fluid in the MSFR core region. In doing this, the use of a uniform hydraulic diameter in the same direction is beneficial from the point of view of numerical stability. Additional friction close to walls can then be added by means of additive-friction-loss coefficients, specified as user input to TRACE, for a more realistic wall drag behaviour. Otherwise, no slip velocity boundary conditions are assumed by TRACE at the walls of *vessel* components.

The last field equations to be solved by TRACE calculates the amount and distribution of DNPs and decay heat in the problem geometry. For DNP group j, the balance equation reads

$$\frac{\partial(\rho c_j)}{\partial t} + \nabla \cdot (\boldsymbol{u}\rho c_j) = \nabla \cdot (D_{m,j}\rho \nabla c_j) + \rho(\beta_j n - \lambda_j c_j), \tag{3.6}$$

where the molecular diffusivity $D_{m,j} = 1.0 \cdot 10^{-3}$ m^{2}s^{-1} for all the groups and for the decay heat in accordance with [Fiorina, 2013] and [Zanetti, 2016], and $j \in \{1, 9\}$, where 9 indicates decay heat. No difference to the balance equation is made when calculating a group of DNPs or decay heat, as the underlying physical processes at work are identical. The group delayed neutron fractions and decay constants were calculated with Serpent using the iterated fission probability method [Leppänen et al., 2014], except for the values for decay heat which were adopted from [Zanetti, 2016]. They are all reported in table 3.1. Compared to traditional DNP balance equations, two additional terms describing convective and diffusive transport of DNPs are introduced in equation 3.6. The equation set is solved by extracting velocity and temperature fields from TRACE in order to evaluate the convection and material properties, respectively. Also part of MSR phenomenology but neglected in the above formulation is DNP extraction through precipitation and deposition. This has been shown to affect less than about 1 % of DNPs [Doligez, 2010].

Group number j	$\boldsymbol{\beta_j}$ **[pcm]**	$\boldsymbol{\lambda_j}$ **[s^{-1}]**
1	22.3	0.0125
2	45.3	0.0283
3	38.8	0.0425
4	60.8	0.133
5	96.9	0.292
6	14.8	0.666
7	20.6	1.63
8	4.49	3.55
Decay heat	253	0.214

Table 3.1: Delayed neutron precursor groups utilised in TRACE calculations.

In addition to the presented field equations, TRACE employs routines for solving heat conduction problems in heat exchangers or through solid heat structures such as fuel pins. These equations are coupled to the field equations above by the term q_w in equation 3.3.

3.1.2 Primary circuit model

The flow path of the MSFR primary circuit has been defined within the aforementioned *vessel* component in TRACE. This was accomplished by taking advantage of the porous media functionality offered by TRACE in *vessel* components to simplify the implementation of channel-like LWR vessels. Porous media functionality allows the user to specify volume fractions taken up by non-fluid (typically solid, internal structures) in each mesh cell, and surface area fractions that are blocked for the fluid on all cell faces. As such, regions of the cylinder-shaped *vessel* component

can be rendered unavailable for the molten salt to enter, and the fluid can thus be directed along the desired flow path. The isolated region represents the blanket and absorber of the benchmark geometry. Although detailed modelling of these parts would be viable, and likely would improve the accuracy of transients particularly sensitive to the large heat reservoirs represented by these compartments, no such modelling has been attempted in this thesis. This simplification is justified in section 4.1.2.

On the top of the *vessel* component, attached to the outermost, torus-shaped cell is a connection that leads to an expansion chamber. Pressure control of the primary is obtained by imposing a boundary pressure at the end of this connection. In transient simulations comparatively cold salt devoid of DNPs enters the primary circuit through from the expansion chamber when the fuel salt contracts. The connection is therefore placed at the core outlet to reduce the neutronic interference of this scenario.

3.1.3 Heat exchanger and pump models

The primary heat exchanger has been modelled in accordance with the recommendations made in a previous study on the topic of MSFR heat exchangers performed at PSI [Ariu, 2014]. Table 3.2 lists the main properties of this heat exchanger.

General properties	
Type	Counterflow printed circuit
Primary side salt	LiF-AcF_4
Secondary side salt	LiF-BeF_2
Length [m]	1.17
Channel shape	Half-circle
Channel diameter [mm]	1.7
Channel pitch [mm]	1.9
Number of channels	253356
Construction material	Hastelloy-N
Primary side properties	
Inlet temperature [K]	1023
Outlet temperature [K]	923
Salt velocity [m/s]	1.17
Pressure loss [bar]	4.1
Secondary side properties	
Inlet temperature [K]	863
Outlet temperature [K]	943
Salt velocity [m/s]	2.00
Pressure loss [bar]	5.2

Table 3.2: Main properties of the implemented primary heat exchanger model, from [Ariu, 2014]. Note that the properties listed describe only one of 16 identical heat exchangers distributed around the MSFR core, and had to be scaled up for use in the axially symmetric benchmark geometry.

On the secondary side, the inlet mass flow rate, temperature, and outlet pressure were imposed in order to obtain the characteristics in table 3.2. Since the properties of the channels were designed for 1/16th the total flow of the MSFR, provisions were made to accommodate the full flow of the axially symmetric model. Specifically, the number of channels and secondary mass flow rate was increased by a factor of 16.

The implemented heat exchanger model stands in contrast to implementations in previous works,

where some simplifications are commonly applied [Zanetti et al., 2015; Fiorina, 2013]. Most importantly, in both cited MSFR models the secondary side temperature is constant and imposed. Heat exchange is then determined by a flow-dependent expression for the heat transfer coefficient between primary and secondary sides.

In TRACE, pumps are modelled as centrifugal pumps in which a rotating impeller imparts momentum to the fluid. The amount of momentum depends on the pump curves used, in addition to the rated torque, rated head, rated volumetric flow, rated fluid density, and rotational velocity of the pump. Throughout this project, all but the latter variables have been set to constant values, and the rotational velocity has been used to vary the primary mass flow. Table 3.3 lists the reference values that have been used to evaluate momentum from a semiscale pump curve built in to TRACE. Also note that the pump is situated above the heat exchanger despite concerns regarding degraded natural circulation, high temperatures, and large thermal stresses in the pump. This design choice follows the convention of the MSFR conceptual drawings in literature [Brovchenko, 2013; Li et al., 2014; Rouch et al., 2014], and deviates from the two other MSFR models previously used for comparison.

Rated head [m^2 s^2]	50
Rated torque [Pa m^3]	3000
Rated volumetric flow [m^3 s^{-1}]	1.0
Rated density [kg m^{-3}]	4125

Table 3.3: Reference values used for evaluating the amount of momentum imparted by the primary centrifugal pump.

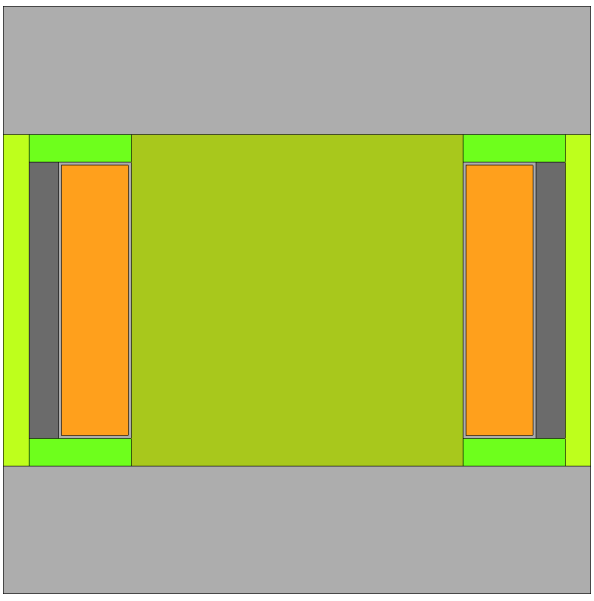

Figure 3.1: MSFR model implemented in Serpent. The different shades of green correspond to different regions in which cross sections were generated. Only the cross sections from the central core region are used in PARCS. The remaining colours represent: orange - blanket, dark grey - absorber, light grey - reflector and blanket casing.

3.2 Serpent

Serpent is a continuous-energy Monte Carlo neutronics code capable of solving the neutron transport problem by tracking individual neutrons within the problem geometry and using stochastic

procedures to determine the chain of events for each neutron. It has been under active development at the VTT Technical Research Centre of Finland since 2004, where it was initially conceived as a tool to simplify group constant generation in a high-fidelity Monte Carlo environment. Since then, Serpent has seen a steady growth of its user base, that now encompasses more than 500 registered individuals in 155 organisations located in 37 countries around the world. This success is not only a result of the simplified cross section generation procedures, but also its high-performance parallel-computation capabilities and user-friendly usage, as well as thorough validation with established codes like MCNP [X-5 Monte Carlo Team, 2003] and experiments.

The MSFR benchmark implementation in Serpent is illustrated in figure 3.1. As in the TRACE model, the geometry is axially-symmetric. Since the heat exchangers and pumps are located behind the neutron absorber where their neutronic importance is severely reduced, their inclusion in the Serpent model has been neglected.

This Serpent model of the MSFR has been used to generate cross sections at a number of different fuel temperatures and densities. By varying these two parameters separately, both individual Doppler and fuel density reactivity coefficients and the combined temperature coefficient could be determined.

Furthermore, reference cross sections were generated at a uniform temperature of 900 K, as well as cross section derivatives to be used by the coupled code in transient analyses. Owing to the fast neutron spectrum of the MSFR, the Doppler cross section derivative for an arbitrary macroscopic cross section x was calculated with [Waltar et al., 2012]

$$\left(\frac{\partial \Sigma_x}{\partial T}\right)_T = \frac{\Sigma_{x,T_1} - \Sigma_{x,T_2}}{\ln T_1 - \ln T_2}, \tag{3.7}$$

while for the fuel density derivatives,

$$\left(\frac{\partial \Sigma_x}{\partial T}\right)_\rho = \frac{\Sigma_{x,T_1} - \Sigma_{x,T_2}}{T_1 - T_2}, \tag{3.8}$$

was used. Note that the reference cross sections were calculated at the temperature of the microscopic cross section libraries used by Serpent closest to the core average temperature (i.e., at 900 K) rather than at the core average temperature itself (about 1030 K) in order to avoid discrepancies introduced by the internal cross section interpolation in Serpent. The derivatives were then calculated using the macroscopic cross sections generated at 900 K and 1200 K.

3.3 PARCS

The Purdue Advanced Reactor Core Simulator is a spatial neutron kinetics solver that calculates the solution to the multi-group neutron diffusion equation, formulated as

$$\frac{1}{v_g}\frac{d\phi_g}{dt} = \nabla \cdot (D_g \nabla \phi_g) - \Sigma_{t,g}\phi_g + \frac{1}{k_{\text{eff}}}\chi_{p,g}\sum_{g'}\nu_{p,g'}\Sigma_{f,g'}\phi_{g'} + \chi_{d,g}\sum_j \lambda_j c_j + \sum_{g'}\Sigma_{g'\to g}\phi_{g'} \tag{3.9}$$

for energy group g, where p denotes prompt neutrons, d delayed neutrons, and j iterates the DNP groups. It does so by discretising the temporal variable according to the theta method, and the spatial variables in a coarse mesh finite difference (CMFD) framework. The resulting finite difference formulation is refined by updating the nodal coupling coefficients by means of a hybrid

nodal expansion and analytical nodal method. For solving steady-state conditions, the eigenvalue problem is then solved using the Wielandt eigenvalue shift method. In transient conditions, the steady-state is first solved and the computed neutron multiplication factor used to make critical the initial state of the transient. A fixed-source problem is established next and solved repeatedly for both the main CMFD equations and local two-node supplementary equations at every point in time of the transient. The use of a diffusion equation formalism is expected to be appropriate for describing the neutron flux present in the large, homogeneous core of the MSFR, provided that a sufficient number of energy groups is defined. That being said, some discrepancies in the flux shape can be expected close to the core boundaries where an albedo boundary condition is used to reproduce the k_{eff} found by Serpent. Specifically, the albedo value set by the user is defined as

$$a_x = \left.\frac{J(x)}{\phi(x)}\right|_{x=x_{\text{surface}}} = \frac{1}{2}\left(\frac{1-\alpha_x}{1+\alpha_x}\right), \text{ where} \tag{3.10}$$

$$\alpha_x = \frac{J_{\text{in},x}}{J_{\text{out},x}}, \tag{3.11}$$

and x_{surface} signifies the radial, top, or bottom boundary. For the radial discretisation in PARCS illustrated in figure 3.2, a value of $a_x = 0.095$ was used on all three boundaries.

Core geometry modelling in PARCS is achieved by defining either square fuel assemblies associated with Western-type LWR cores, or hexagonal assemblies for VVER-type cores. Thus, for coupling purposes, the number of assemblies specified in PARCS must be high to obtain a good approximation of the cylindrical mesh used in TRACE. Since fewer hexagonal assemblies are required to obtain a good approximation of a circle than squares, the hexagonal shape was chosen to reduce the computational burden. Figure 3.2 shows an example of a radial mesh used in PARCS. In the axial direction, the discretisation from TRACE could be directly adopted.

Collapsed and spatially averaged macroscopic cross sections generated in the core region by Serpent were provided to PARCS. For this purpose, a six-group energy discretisation was adopted from previous studies on the MSFR neutronic behaviour [Zanetti, 2016; Fiorina, 2013; Aufiero, 2014]. Table 3.4 recalls the particular discretisation. In addition to this, cross section derivatives were calculated from Serpent calculations performed at 900 K and 1200 K, corresponding to the temperatures of the microscopic cross section libraries used by Serpent. By providing a reference fuel and coolant temperature, PARCS evaluates the differences with regards to current cell temperature and uses linear extrapolation to continuously update the cross sections throughout the transient calculation. Since PARCS also receives the DNP concentrations, c_k from TRACE, it is able to solve equations 3.9 for the neutron group fluxes and return the associated power distribution.

Group number	1	2	3	4	5	6
Lower boundary [MeV]	2.231	$4.979{\cdot}10^{-1}$	$2.479{\cdot}10^{-2}$	$5.531{\cdot}10^{-3}$	$7.485{\cdot}10^{-4}$	0

Table 3.4: Lower boundary of the energy groups utilised in PARCS calculations.

3.4 Coupling methodology

The coupling between TRACE and PARCS is accomplished by mapping thermal-hydraulic cells in TRACE to corresponding neutronic nodes in PARCS. One such map of radial nodes is illustrated in figure 3.2. In the axial direction, one-to-one mapping is used. Cell fluid temperatures and densities are then transferred from TRACE to PARCS through an interprocess communication protocol. Moreover, source code extensions to allow for the transfer of DNP concentrations have been implemented at PSI, and further extended to be compatible with *vessel* components within this project.

From the temperature and DNP distributions, PARCS calculates the cell-wise power distribution, which is then returned to TRACE. Originally, the calculated power distribution is returned to solid heat structure components in TRACE representing the fuel rods in LWRs. Additional modifications to the TRACE source code have been made at PSI in the past to ensure that the returned power is deposited directly in to the coolant [Kim, 2015], as is the case for liquid-fuelled reactors.

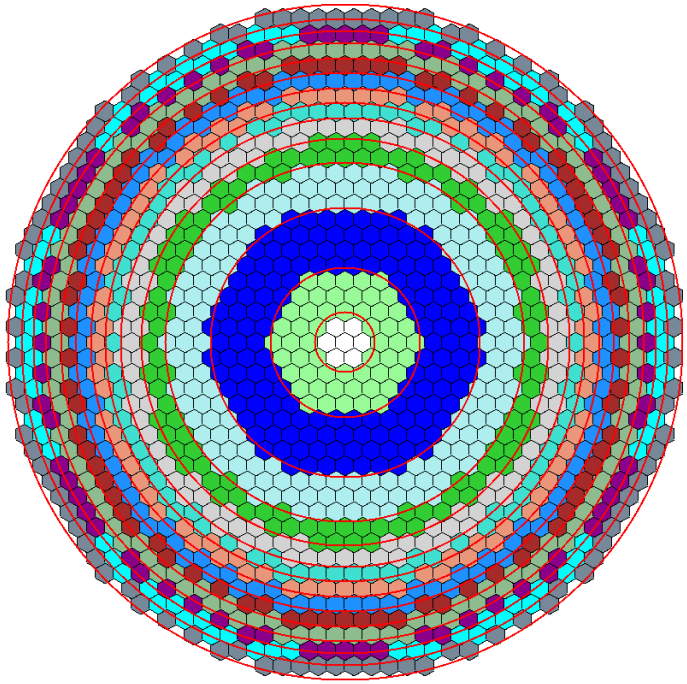

Figure 3.2: The radial discretisation of the MSFR core (inner salt circle in figure 2.2b) in PARCS overlaid with the TRACE discretisation (red, circular lines) illustrating the coupled regions that map variables from one code to the other. In total, 1285 radial cells have been used in PARCS to cover the 14 radial core cells in TRACE.

Throughout the coupled calculation the two codes are run in parallel, and the aforementioned information exchange procedure is performed at every time step. This coupling approach is called operator splitting, and has the advantage of being very intuitive, and allowing two well-established and thoroughly validated codes to operate together in a coupled manner. Conversely, operator splitting is time consuming as one code always has to await the response of the other, and suffers from issues of numerical stability related to the control of the size of time steps [Pope and Mousseau, 2009]. In TRACE, a variable time step control procedure determines at any time the appropriate time step size subjected to upper and lower boundaries imposed by the user. To reduce computational times, this time-differencing procedure is allowed to exceed the material Courant limit condition that relates the time step size to the characteristic cell size and fluid velocity [NRC, 2007]. Generally, this routine was found to be unreliable for coupled calculations, and a strict restriction on the upper time step size had to be given to ensure stability.

4 Results

Two main categories of simulations have been performed over the course of this project. First, the neutronic and thermal-hydraulic steady-states of the MSFR were separately investigated using Serpent and TRACE, respectively. Of these, Serpent was run first in order to determine the power distribution and DNP properties later provided to TRACE. Furthermore, macroscopic cross sections generated by Serpent were used in the standalone PARCS code, and the resulting neutronic solution has been compared with that of Serpent. Second, TRACE and PARCS have been coupled in order to study transient behaviour. Specifically, transients describing primary pump over-speed, primary circuit over-cooling, loss of heat sink, and loss of flow scenarios have been investigated.

Results from both the steady-state and transient simulations are presented in the following. Since obtaining steady-state simulations in both TRACE and PARCS are prerequisites for performing coupled calculations, it is natural to begin with the steady-state. In both cases, the obtained results have been compared with results from other tools where data is available. This includes an ERANOS-based code [Fiorina, 2013; Rimpault et al., 2002] used for steady-state neutronic assessments, and a CFD tool [Fiorina, 2013] based on the physics simulator COMSOL [COMSOL, 2012] and the DNP-extended TRACE code with a simplified point-kinetics routine (hereby referred to as TRACE-PK [Zanetti, 2016]), both used for steady-state thermal-hydraulic and transient analyses.

It should be noted that because of the interconnected structure of the computational procedures followed, almost all presented results will have some dependency on the microscopic cross section library providing data to Serpent. Unless otherwise specified, the JEFF 3.1.1 library [Santamarina et al., 2009] has been used.

4.1 Steady-state behaviour

The steady-state behaviour of the MSFR has been characterised both in terms of neutronics and thermal-hydraulics, in an uncoupled manner. There are two main incentives for doing this. First, the steady-state solution is required in order to initialise the coupled tool that serves as the focal point of this thesis. Second, the steady-state analysis highlights a number of characteristics of MSRs in general, and the MSFR in particular. Thus, the presented results and associated discussion aims at clarifying and expanding some of the concepts previously introduced, and provide context for interpreting the transient results that follow.

For performing steady-state simulations, some assumptions had to be made that limit the accuracy of the obtained results. Most importantly, the neutronic study using Serpent was performed at uniform fuel salt temperatures, and the thermal-hydraulics were studied with an imposed, time-invariant power distribution obtained from the uniform-temperature Serpent model. As a result, in terms of thermal-hydraulics, discrepancies can be expected compared to the COMSOL and TRACE-PK tools that both make use of a power distribution calculated by means of a spatial neutron diffusion approach. Justification for introducing this additional source of discrepancy lies

in that the main focus of this work is the assessment of the coupled TRACE-PARCS tool. Separate-physics simulations of the thermal-hydraulic steady-state behaviour are merely a necessary step for initialising the transient simulations performed with the coupled tool, for which this limitation is lifted.

In the following, the neutronic steady-state will first be described. This includes results obtained with Serpent, as well as comparisons with standalone PARCS and similar results from literature. Thereafter, a brief study of nominal power deposition in the blanket is presented in an attempt to justify the choice of neglecting the blankets in the thermal-hydraulic model. Finally, the TRACE steady-state solution will be presented and compared with the CFD-based COMSOL and TRACE-PK solutions where possible.

4.1.1 Neutronics

The steady-state neutronic results presented in the below were obtained by following a particular computational procedure. First, Serpent was used to calculate k_{eff} at a uniform temperature corresponding to a preliminary estimate of the core average temperature of 1030 K.[5] The amount of fissile material was then adjusted in order make the reactor critical at this temperature. This resulted in a 1 % increase compared to the benchmark reference fissile inventory [Merle-Lucotte et al., 2011], but also a 2 % decrease compared to the values reported in [Fiorina, 2013]. Next, macroscopic cross sections were generated from simulations at temperatures of 900 K (used as reference) and 1200 K (for calculating derivatives). At the latter temperature two sets of simulations were performed in order to separate the effects from changes of fuel temperature and fuel density. At the same time, k_{eff} was calculated in order to evaluate the two feedback coefficients, as well as the combined temperature coefficient.

By following the procedure outlined in [Ghasabyan, 2013], cross sections calculated by Serpent can be introduced into PARCS. This opens up for two distinct methods of performing PARCS calculations at different core temperatures, namely (a) to use directly cross sections generated at the desired temperature, or (b) using reference cross section together with cross section derivatives. Only the second method is compatible with spatial temperature distributions, and has therefore been used in the following. The only exception to this rule was made when calibrating the PARCS boundary conditions to correspond with results from Serpent. That is, the albedo condition was adjusted to yield a critical core at the uniform core temperature of 1030 K using Serpent cross sections generated at 1030 K. Then, method b could be used to evaluate k_{eff} at different temperatures and compare the resulting temperature coefficients with Serpent, which was adopted as reference. The results are reported in tables 4.1 and 4.2, for three different numbers of radial cells in PARCS, together with values from ERANOS where appropriate.

Code	$k_{\text{eff, 1030 K}}$	**Diff. wrt. Serpent [pcm]**	$k_{\text{eff, 1200 K}}$	**Diff. wrt. Serpent [pcm]**
Serpent	1.00000	0	0.98716	0
PARCS, 2929 cells	0.99917	-83	0.98633	-83
PARCS, 1891 cells	0.99917	-83	0.98625	-91
PARCS, 1285 cells	0.99917	-83	0.98624	-92

Table 4.1: Selected values of k_{eff} as calculated by the different tools. The number of cells in PARCS refer to radial cells (c.f. figure 3.2).

[5] This estimate was in turn obtained by using a first-approximation cosine-shaped power distribution in TRACE.

Code	α_D [pcm/K]	α_ρ [pcm/K]	$\alpha_D + \alpha_\rho$ [pcm/K]	α_T [pcm/K]
Serpent	-3.88 ± 0.02	-3.48 ± 0.02	-7.36 ± 0.03	-7.27 ± 0.02
PARCS, 2929 cells	-3.87	-3.54	-7.41	-7.58
PARCS, 1891 cells	-3.87	-3.59	-7.45	-7.62
PARCS, 1285 cells	-3.87	-3.59	-7.46	-7.63
ERANOS	-4.19	-3.10	-7.29	N/A

Table 4.2: Reactivity coefficients as calculated by different tools. The number of cells in PARCS refer to radial cells (c.f. figure 3.2). See the nomenclature for explanation of symbols. For all but the bottom row, the coefficients have been calculated as $\alpha = (k^2_{\text{eff}} - k^1_{\text{eff}})/(k^1_{\text{eff}} \cdot \Delta T)$, with $k^1_{\text{eff}} = k_{\text{eff}}(900\text{K})$, $k^2_{\text{eff}} = k_{\text{eff}}(1200\text{K})$, and $\Delta T = (1200 - 900)$ K. In the ERANOS calculations, 973 K and 1073 K were used in place of 900 K and 1200 K [Fiorina, 2013].

A few conclusions can be drawn from tables 4.1 and 4.2. First, differences in k_{eff} between PARCS and Serpent are on the order of 100 pcm, and do not vary much with the number of radial cells in PARCS. Second, the assumption that the overall temperature reactivity coefficient, α_T, is a superposition of the Doppler and fuel density coefficients appears good with discrepancies on the order of 1-2 %. Third, the discrepancies between PARCS and Serpent for the summed Doppler and density coefficients (which are the ones used in PARCS)) are also about 1-2 %, and only modest improvements are obtained with considerably more radial cells. This could likely be improved by increasing the number of zones in which Serpent produce cross sections for PARCS. However, that is not done here as these results are deemed acceptable for the purpose of verifying code behaviour. Also, in order to reduce computing times without sacrificing much accuracy, the roughest radial mesh is chosen in PARCS for the continued analysis. Fourth, both PARCS and Serpent results are consistent with those from ERANOS. The discrepancy in the Doppler coefficient is likely due to the aforementioned difference in fuel composition [Fiorina, 2013], while the fuel density coefficient could be related to the extrapolation of the salt density used when calculating k_{eff} at 1200 K (c.f. table 2.2). In the ERANOS calculations this was avoided by calculating the coefficients between 973 K and 1073 K, which, on the other hand, introduces uncertainty related to microscopic cross section interpolation.

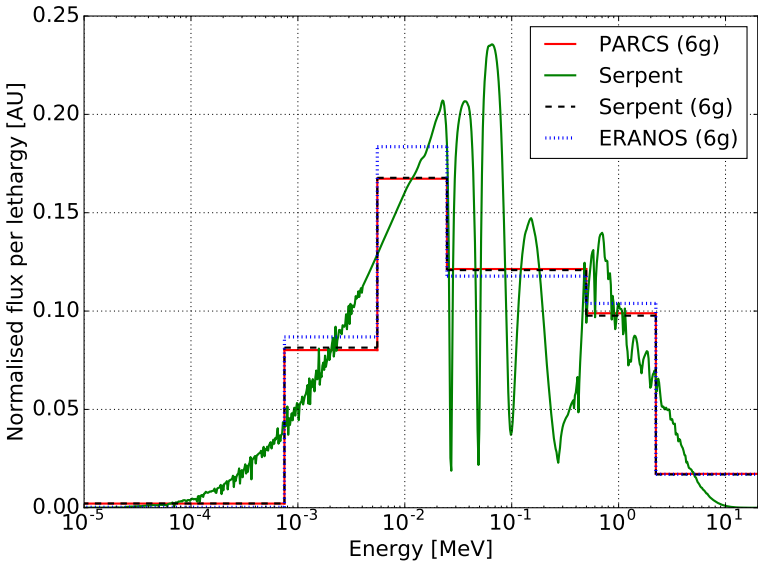

Figure 4.1: Neutron energy spectrum for the MSFR as calculated by Serpent, PARCS (using cross sections from Serpent), and ERANOS [Fiorina, 2013].

Next, PARCS was used to calculate the spatial power distribution and energy spectrum at a uniform

core temperature of 1030 K. Figure 4.1 compares the neutron spectra calculated by PARCS and Serpent at this temperature with results from ERANOS calculated at 973 K, while figures 4.2 and 4.3 compare radial and axial power distributions, respectively, in PARCS and Serpent.

As can be seen, the MSFR features a fast neutron spectrum with distinct flux depressions corresponding to elastic scattering resonances in fluorine and lithium. In comparison with Serpent, PARCS can be seen to excellently reproduce the collapsed neutron flux spectrum, which is a bit softer than the one from the ERANOS calculations. This is due to the lower fissile inventory in this study compared to that of [Fiorina, 2013].

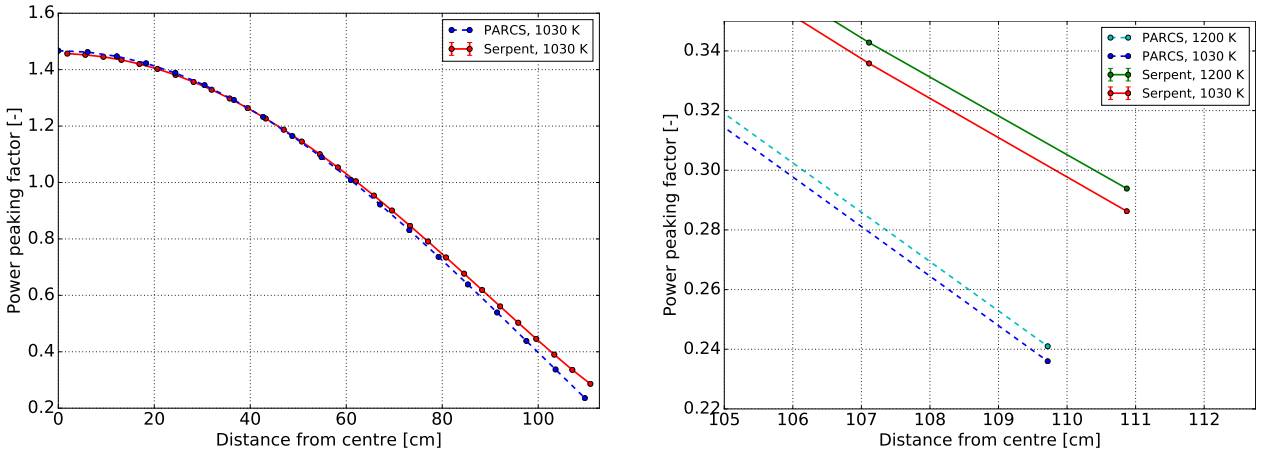

(a) (b)

Figure 4.2: Radial power distributions as calculated by Serpent and PARCS, **(a)** at a uniform fuel temperature of 1030 K, and **(b)** close to the core periphery at uniform fuel temperatures of 1030 K and 1200 K. Evidently, both codes predict increased leakage as the temperature is increased and the spectrum hardens. The uncertainties of the Serpent calculations represent one sigma, and are too small to be resolved on these axes.

Figures 4.2 and 4.3 show the radial and axial power peaking factors, respectively. Considering the fundamentally different solution methodologies, in addition the the coarse energy discretisation employed by PARCS, the spatial resemblance between PARCS and Serpent is quite good. Also, as can be seen in figure 4.2b, an increase in fuel salt temperature leads to increased leakage as the spectrum hardens slightly. Both codes reproduce this behaviour. Some discrepancy exists close to the boundary, and is due to the simplified albedo condition imposed in PARCS. No visible improvements are evident when going to more radial PARCS nodes, as was the case for the reactivity coefficients. The agreement would likely be improved by calculating the albedo on all sides of the core using Monte Carlo simulations, as well as increasing the number of zones in the core in which cross sections are generated with Serpent. Again, for the purpose of assessing the coupled tool, this was not deemed necessary.

It is not possible to directly specify core temperature in PARCS when using derivatives. Thus, in order to perform the reported PARCS calculations at variable, uniform temperatures, the coupling with TRACE was taken advantage of by preparing thermal-hydraulic, zero-power simulations of stagnant fuel salt. A natural progression from this is to give PARCS the distributed temperature field from full-power TRACE simulations at steady-state. For both of these cases, k_{eff} has been calculated using the reference cross section at 900 K and derivatives. Table 4.3 reports these findings.

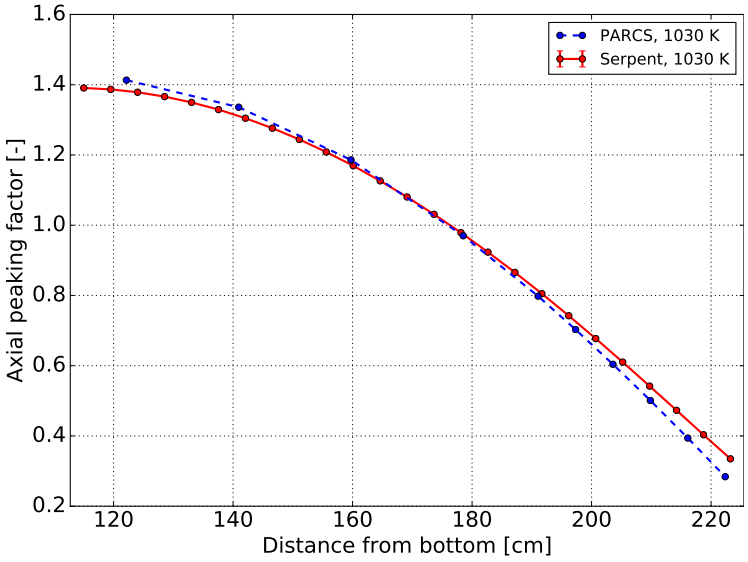

Figure 4.3: Axial power distribution as calculated by PARCS and Serpent at a uniform core temperature of 1030 K. The uncertainties of the Serpent calculations represent one sigma, and are too small to be resolved on these axes.

Temperature distribution	$T_{\text{core, avg.}}$ **[K]**	k_{eff}
Uniform, 1030 K cross sections	1030	1.0
Uniform, derivatives	1030	0.99917
Distributed	1034	1.00032

Table 4.3: Neutron multiplication factors calculated by PARCS with different cross section and temperature input.

As can be seen, differences on the order of 80 pcm are observed when cross section interpolation with derivatives is used. This indicates a more complex cross section dependency with temperature, but could also be influenced by the microscopic cross section interpolation in Serpent. The change to distributed temperatures introduces 115 pcm of positive reactivity despite increasing the core average temperature by about 4 K. Much of the reason for this is the existence of a localised region of high salt temperatures outside of high neutron importance regions in the centre of the core (c.f. chapter 4.1.3).

A final note is offered on the use of microscopic cross section libraries in Serpent. Although JEFF 3.1.1 is used exclusively in this thesis, k_{eff} at 900 K was calculated using the ENDF/B-VII library [Chadwick et al., 2011] with Serpent. A difference of more than 1000 pcm was found, with ENDF providing the more conservative estimate. This is consistent with other reports of important dependency on cross section libraries, primarily due to uncertainties in the (n, γ) capture cross section of ^{233}U [Aufiero, 2014].

4.1.2 Blanket behaviour

The amount and distribution of power deposited in the blanket during steady-state operation was investigated in order to advise the thermal-hydraulic modelling of the MSFR primary circuit. In particular, the study was aimed at determining the importance of including a detailed blanket model for the steady-state thermal-hydraulic analysis.

Two main phenomena are responsible for heating the blanket. At beginning of life, when only

thorium is present in the blanket, gamma heating is the dominant factor. However, as ^{233}U is bred, fissioning begins contributing to the power deposition as well. In general, the total power production will increase as ^{233}U reaches its equilibrium concentration. For this reason, an equilibrium blanket salt composition is adopted [Brovchenko, 2013] to avoid excessive non-conservatism. The combined neutron and photon transport problem is then solved using the Monte Carlo code MCNP6 [Pelowitz et al., 2014]. Figure 4.4 shows the resulting power deposition profile, while table 4.4 lists the total power deposited

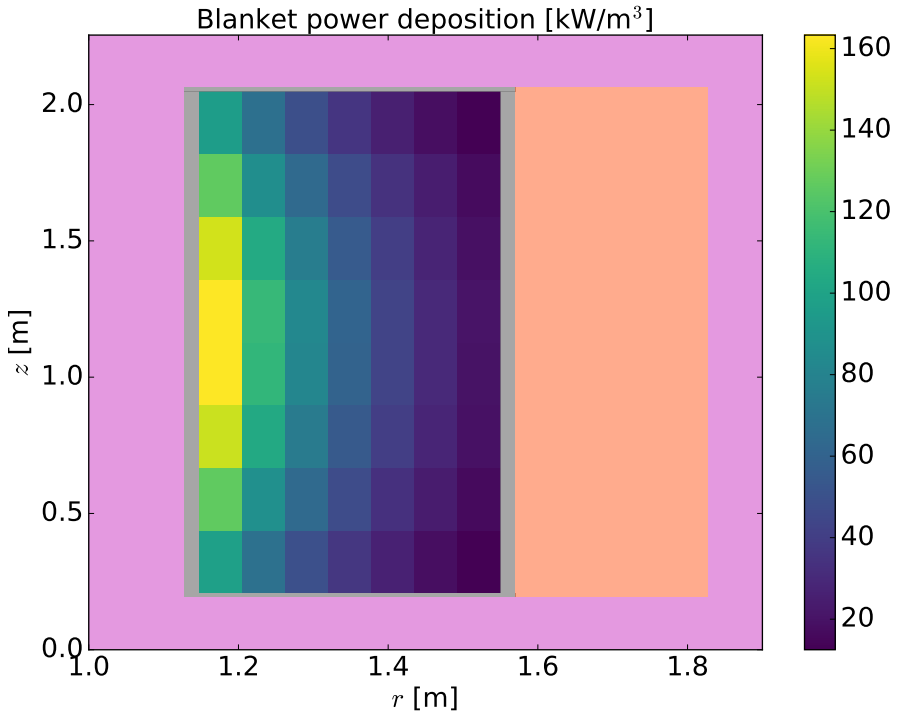

Figure 4.4: Distribution of power deposition in the blanket as calculated by MCNP.

Process	**Power [MW]**
Gamma heating	10.2
Neutron heating	11.0
Sum	21.2

Table 4.4: Total power deposition in the blanket from gamma and neutron heating.

The total power deposition of 21.2 MW is in good agreement with similar studies [Rouch et al., 2014], albeit somewhat lower as decay heat is not accounted for. Compared to the nominal core power of 3000 MW, blanket heating is negligible and can safely be ignored in steady-state calculations of the primary circuit. On the other hand, it is clear that active cooling is required to dissipate this and potential heat transfer from the fuel salt in a controlled fashion. Furthermore, under transient conditions the blanket will represent an important heat repository that will affect the temperature evolution of the primary circuit. In the transient analysis performed in this work no such effects have been included, and simplicity of the model has been prioritised. It is, however, identified as a topic that will require future investigation.

4.1.3 Thermal-hydraulics

By introducing the DNP parameters and power distribution computed by Serpent in to the MSFR model in TRACE, it has been possible to investigate steady-state thermal-hydraulic behaviour of

the benchmark MSFR problem, in addition to the DNP distribution. In the following, some remarks on the model and methodology will be given, followed by the presentation of selected results. These include the steady-state velocity, temperature, and pressure fields, as well as DNP distributions and the effective delayed neutron fraction, β_{eff} (which are not thermal-hydraulic results, per se, but computed by the thermal-hydraulic code).

Due to the simplified coarse-mesh approach utilised by TRACE, it has been of particular interest to compare the obtained results with those from a more complex, CFD-based solver implemented in COMSOL. This tool is explained in detail in [Fiorina, 2013]. Some model adjustments were required in order to facilitate this comparison. Specifically, the inlet and outlet temperature of the core were aligned with those of the COMSOL solution, which did not correspond exactly to the benchmark values. Most importantly, the temperature rise in the core was close to 90 K instead of 100 K. Furthermore, it was found that adding artificial friction in the core region as described in chapter 3.1 improved mixing and thus the distribution of heat. As such, the core peak temperature could be made the same as in the COMSOL model.

Steady-state was obtained in approximately ten minutes on a single 2.6 GHz Intel Xeon processor. Most of this time was taken up by the convergence of the DNPs - the half-life of the longest-lived group is about 50 s, so simulation times had to exceed five times this as a minimum. The thermal-hydraulics solution in itself converged much faster, in the order of tens of seconds. Initially, efforts were directed towards modelling the full three-dimensional geometry in TRACE by subdividing the cylindrical mesh into 16 azimuthal sectors representing the individual recirculation loops. This was desirable as it would allow for the simulation of asymmetrical transients such as single pump failure. However, computational times were found to scale significantly with model complexity, especially for the coupled tool, to the point that simulations on a single processor was unfeasible. It should be noted that parallelisation is possible in TRACE by decomposing the model into zones that are solved on separate processors, but the process is not straightforward and was not attempted in this thesis work.

An important aspect of any numerical method that requires discretisation of the spatial variables is the selection of computational mesh. The mesh chosen for this work is based on the mesh used in the TRACE-PK model [Zanetti, 2016], with some additional refinement in the axial direction close to the core inlet and outlet to allow for additional wall friction modelling. Furthermore, the outermost radial cell was chosen in order to simplify the implementation of the primary pump and heat exchanger. With this mesh, mesh independence was not achieved. When increasing the total amount of cells by a factor of three, keeping all other settings the same, salt mixing in the core is degraded and the peak temperature increases by 11 %, corresponding to 140 K. However, by readjusting friction values in the core, the smaller-mesh steady-state solution can be retrieved. It can be concluded that some amount of model calibration with an alternative solution is required for the successful application of this tool. In the opposite direction, when fewer cells are used, the steady-state solution can not be obtained, thus indicating a good optimisation in terms of minimising computational requirements.

Velocity field

The alignment of the core inlet and outlet temperatures with the COMSOL solution was achieved by adjusting two parameters. Inlet temperature was controlled by specifying the mass flow rate on the secondary side of the heat exchanger, and the outlet temperature by the rotational speed of the primary pump. When the two solutions coincided, primary mass flow rate had been increased to about 23800 kg/s, up almost 30 % compared to the benchmark value of 18500 kg/s. This discrepancy is mainly explained by differences in the specific heat capacity (a minor influence comes from the core temperature increase being 90 K rather than 100 K). While this work has considered the more conservative average value over the experimental range in table 2.2, COMSOL

extrapolates the given expression to the temperatures of the MSFR. As a result, it operates with a higher c_p than TRACE. If c_p is extrapolated also in TRACE,[6] the benchmark values for mass flow rate, power, and temperature increase in the core are retrieved.

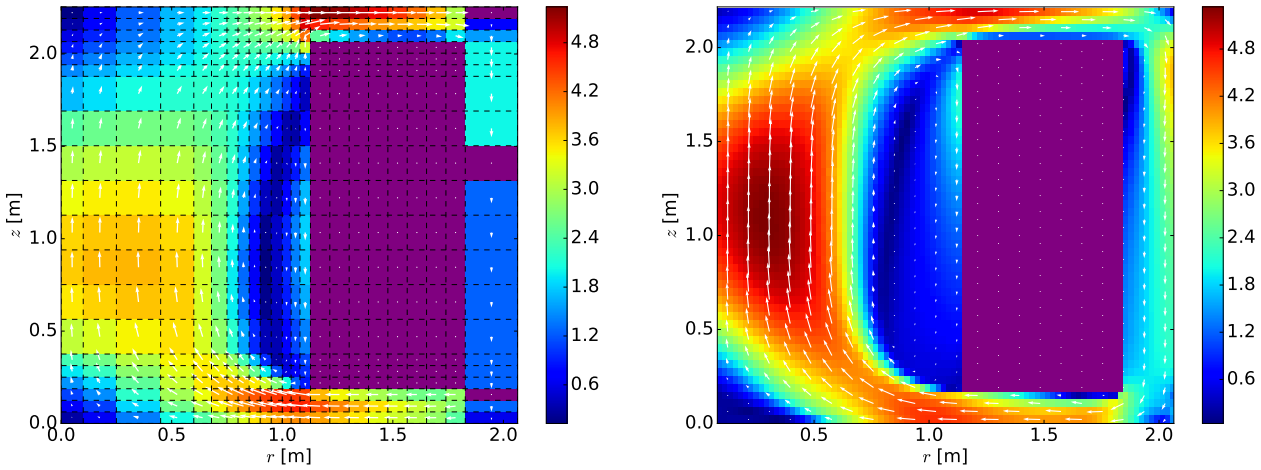

(a) (b)

Figure 4.5: MSFR velocity field [m/s] as calculated by **(a)** TRACE and **(b)** COMSOL.

The flow fields produced by TRACE and COMSOL are reported in figure 4.5. Both are characterised by a large recirculation zone of nearly stagnant salt close to the boundary with the blanket tank. The size of the zone is predicted to be larger in COMSOL, so that also the salt velocity across the remainder of the flow area is greater than predicted by TRACE. Other main features such as the two additional stagnant zones located at the top and bottom of the centre of the core are calculated by both codes. Evidently, TRACE is not able to reproduce the same level of detail as that of the COMSOL simulation. However, considering that TRACE is ignoring all turbulence effects, the agreement is reassuringly good.

One consequence of the recirculation zone is that part of the primary salt volume is restricted from circulating. As a result, the transit time of the remaining salt is reduced and can no longer be evaluated as the ratio of salt volume to volume flow. Instead, the transit time has been evaluated by depositing DNPs in a single cell in a single time step and counting the time between two subsequent peaks in DNP concentration. The transit time was thus found to be 2.9 s. Similar simulations in COMSOL and TRACE-PK yield values of 3.1 s and 3.75 s, respectively, where the latter is reproduced in TRACE when the nominal mass flow rate is used.

Temperature field

Figure 4.6 plots the steady-state temperature fields calculated by TRACE and COMSOL. From these plots, a second consequence of the large recirculation zone is readily observable, as temperatures in the stagnant salt peaks more than 200 K above the temperature of the surrounding fuel salt. This translates into excessive thermal stresses on structural components such as the blanket tank, and constitutes a major incentive for exploring alternative core geometries with reduced salt stagnation and straighter streamlines [Li et al., 2014; Aufiero et al., 2014; Rouch et al., 2014].

[6] It has not been possible to implement the table 2.2 expression for c_p in TRACE. Instead, a constant value evaluated at the mid-point of the benchmark inlet and outlet temperatures is used.

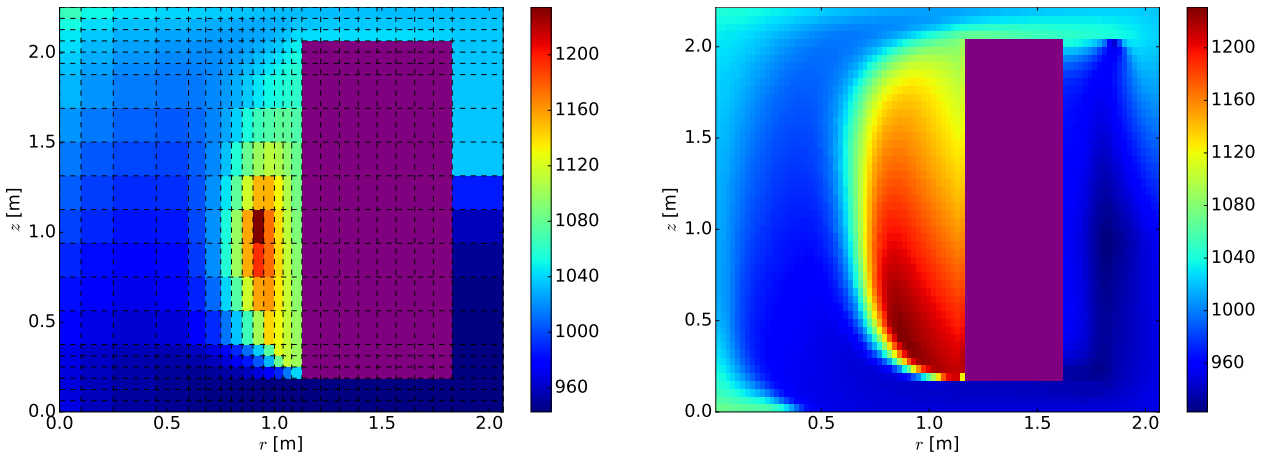

(a) (b)

Figure 4.6: MSFR temperature field [K] as calculated by **(a)** TRACE and **(b)** COMSOL.

TRACE is able to reproduce the main trends of the COMSOL temperature solution, with the exception of the hot spot in the bottom, central part of the core which is much more pronounced in COMSOL. The larger size of the recirculation zone predicted by COMSOL results in a larger hot spot, with a more distributed peak temperature than in TRACE. As a consequence, also the average core temperature is higher in COMSOL. It is found to be 1073 K and 1034 K in COMSOL and TRACE, respectively. Also of note is the different temperature distributions in the vertical part of the recirculation loop. This is because TRACE has the pump above the heat exchanger, while the reverse is true in the COMSOL model.

Pressure field

The pressure distribution calculated by TRACE, reported in figure 4.7, is dominated by the pressure head generated by the pump, and primarily lost in the heat exchanger. In fact, owing to the elevated primary mass flow rate, both the salt velocity inside and pressure loss over the heat exchanger are slightly greater than the reference values given in table 3.2, with magnitudes of 1.25 m/s and 4.35 bar. If the mass flow is reduced to near nominal values, the pressure loss over the heat exchanger is approximately the same as in the COMSOL and TRACE-PK models, where it has been imposed as 3 bar at nominal conditions. Contributing factors to the pressure field beyond the pump and heat exchanger are the hydrostatic pressure creating a vaguely discernible gradient from top to bottom, and the expansion vessel, connected to the outermost cell on the top of the reactor model, in which a pressure of 4.5 bar is imposed in accordance with the TRACE-PK model.

It should be mentioned that actual pressure losses will most surely be higher than the predictions made with this model. This is because only frictional losses from wall drag has been taken into account, albeit in abundance in order to emulate viscous shear stresses. Important sources of head loss that have been ignored include abrupt flow area change losses such as those encountered in the heat exchanger, as well as losses in pipe bends, elbows, and the like.

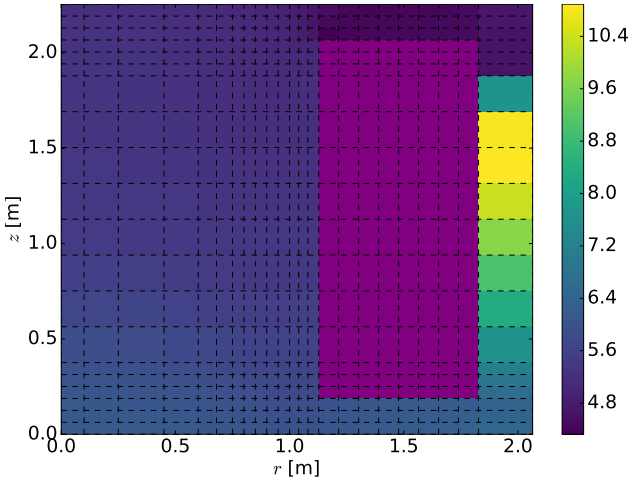

Figure 4.7: MSFR pressure field [bar] as calculated by TRACE.

DNP field

The unconventional behaviour of the DNPs in liquid-fuelled reactors is easily recognisable in figures 4.8a-4.8i which display the steady-state spatial concentration of the eight DNP groups and the decay heat deposition. Whereas longer-lived precursors are circulated multiple times and distributed near-uniformly in the primary circuit, the concentration of progressively shorter-lived DNPs approach the power distribution. In the case of DNP group 8 with a half-life of only 0.2 s, the distribution is nearly the same as the power distribution, only slightly shifted upwards with the flow. The obtained distributions comply both with intuition and with results from the CFD-based tool from TU Delft [van der Linden, 2012].

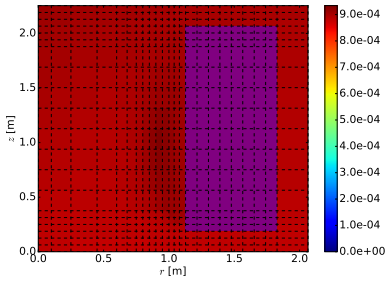

(a) Group 1: $T_{1/2} = 55.6$ s.

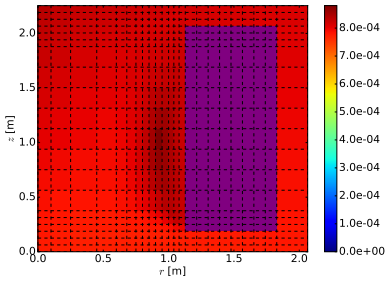

(b) Group 2: $T_{1/2} = 24.5$ s.

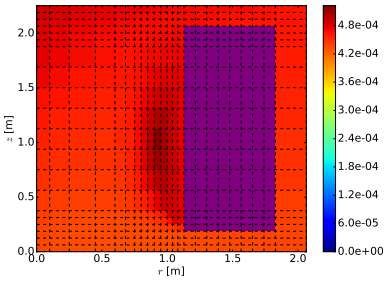

(c) Group 3: $T_{1/2} = 16.3$ s.

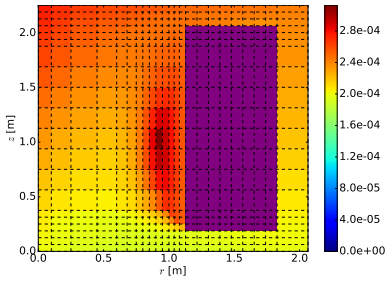

(d) Group 4: $T_{1/2} = 5.2$ s.

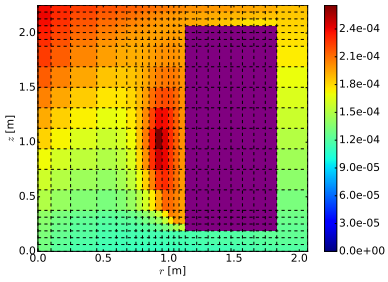

(e) Group 5: $T_{1/2} = 2.4$ s.

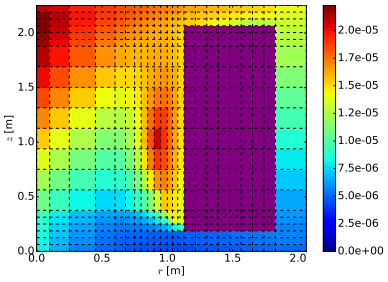

(f) Group 6: $T_{1/2} = 1.0$ s.

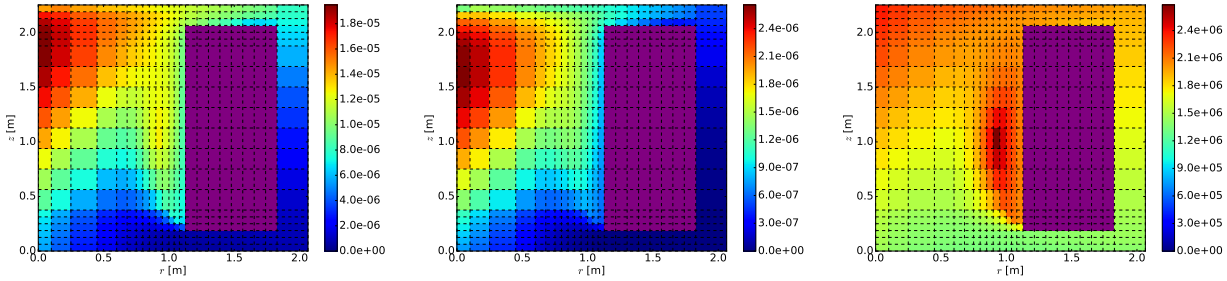

(g) Group 7: $T_{1/2} = 0.4$ s. (h) Group 8: $T_{1/2} = 0.2$ s. (i) Decay heat: $T_{1/2} = 3.2$ s.

Figure 4.8: Normalised DNP concentrations for the eight DNP groups and decay heat as calculated by TRACE. Values in W/m^3 for the decay heat, and arbitrary units for the others. Note that the upper limits of the colour legends differ from one plot to another.

An important concept for reactor control is the fraction of delayed neutrons, commonly denoted β. This concept is extended to the effective delayed neutron fraction, β_{eff}, by taking into account the ability of the delayed neutrons to initiate new fission processes. For solid-fuelled reactors, the main source of discrepancy between β and β_{eff} is the energy spectrum of the delayed neutrons which generally differs from the prompt neutron spectrum. In liquid-fuelled reactors, the position of precursors in the primary circuit constitute another essential influence. As an example, the neutronic importance of a delayed neutron born inside the heat exchanger is nil.

The effective delayed neutron fraction for DNP group i can be calculated as [Aufiero, 2014; Mattioda et al., 2000]

$$\beta_{\text{eff},i} = \frac{\int \phi^* \lambda_i c_i}{\int \sum_j \phi^* \lambda_j c_j + \int \phi^* \nu \Sigma_f \phi}, \tag{4.1}$$

where ϕ^* represents the adjoint flux, j iterates the DNP groups, and the integral is over space and energy. For the steady-state solution in TRACE, only the power distribution is known. However, for a critical reactor at steady-state, the power deposition correlates well with neutron flux, which is assumed to sufficiently resemble the adjoint flux for the purposes of this work. Obviously, since β_{eff} then depends on recirculation time, power distribution, DNP concentration, core flow field, as well as fuel composition (affecting β) it represents an excellent figure-of-merit for comparing the ability of different codes to calculate liquid-fuel steady-state behaviour. Table 4.5 presents one such comparison between TRACE, TRACE-PK, and COMSOL.

Code	$\beta_{\text{eff,static}}$ **[pcm]**	$\beta_{\text{eff,moving}}$ **[pcm]**								
		1	2	3	4	5	6	7	8	**Sum [pcm (%)]**
TRACE	303.6	7.5	15.4	13.3	21.3	35.4	6.1	11.3	3.3	113.7 (37.4)
TRACE-PK	318.1	9.1	17.9	15.6	24.5	40.5	7.1	13.8	3.8	132.1 (41.5)
COMSOL	318.1	9.2	18.2	16.2	25.9	42.9	7.4	12.9	3.6	136.3 (42.8)

Table 4.5: β_{eff} in the three different codes. A distinction is made between $\beta_{\text{eff,static}}$ that only take into account spectral effects, and $\beta_{\text{eff,moving}}$ that also includes DNP transport. The sum is given both in absolute terms, and as a fraction of the static fuel value.

Both TRACE-PK and COMSOL give very similar results since they use the exact same power distribution (as determined by COMSOL), and the same value for $\beta_{\text{eff,static}}$. The value for $\beta_{\text{eff,static}}$

used in TRACE was calculated with Serpent for the fuel composition with a lower fissile content than for the other models.

Nevertheless, when the relative size of $\beta_{\text{eff, moving}}$ to $\beta_{\text{eff, static}}$, hereby referred to as the circulation correction factor, cf_{circ}, is compared, TRACE is still found to produce a lower estimate. Part of the reason for this is the elevated mass flow that was required in order to reproduce the core inlet and outlet boundary conditions from COMSOL. Indeed, when plotting cf_{circ} as a function of mass flow rate (cf. figure 4.9), it is clearly seen that an increase in mass flow rate is correlated with a reduction of delayed neutrons in the core, primarily from the shorter-lived DNP groups. At the nominal mass flow rate of 18500 kg/s, $cf_{\text{circ}} \approx 38.5$ %. The remaining discrepancy is likely a result of the difference in power distributions and the larger recirculation zone in COMSOL that helps to increase the number of DNP decays that occur in the core.

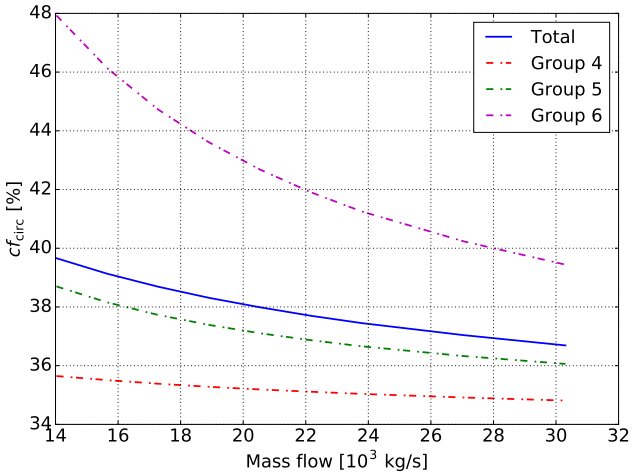

Figure 4.9: The circulation correction factor for DNP group j, $cf_{\text{circ},j} = \frac{\beta_{\text{eff, moving},j}}{\beta_{\text{eff, static},j}}$, for selected groups and the total effective DNP fraction, as a function of the primary mass flow rate.

4.2 Transient behaviour

The strong interdependence between neutronics and thermal-hydraulics exhibited by liquid-fuelled reactors necessitates the use of multi-physics tools for studying time-dependent behaviour. In this work, transient analysis of the MSFR has been realised by coupling TRACE with PARCS so that temperature, DNP, and power deposition fields are exchanged between the two codes. In the coupled tool, PARCS operates with macroscopic cross sections and associated derivatives calculated with Serpent in order to model the strong temperature feedbacks present in the MSFR. To the author's knowledge, this represents only the second application of the coupled TRACE-PARCS code to an MSR (the first being [Kim, 2015]), and the first in which a multi-dimensional thermal-hydraulics geometry is modelled.

On account of the novelty of these simulations, it has been necessary to conduct an assessment of the ability of the coupled code to reproduce the dynamic behaviour of the MSFR. To that end, the results presented in the following have been compared with similar computations performed with the TRACE-PK and COMSOL tools. It should be noted that since no experimental data exists for the MSFR also the reference solutions should be approached with a certain level of skepticism. In this way, the objective of this work is code verification rather than validation, that is, to ensure that the results are in accordance with model expectations.

Prior to simulating dynamic behaviour, a particular procedure for initialising the coupled calculations had to be followed. The specificities of this procedure are detailed in appendix A. In this

chapter, the results from four different transient investigations are presented and compared with corresponding TRACE-PK and COMSOL results. These are (1) unprotected[7] loss of heat sink (ULOHS), (2) unprotected pump over-speed (UOS), (3) unprotected over-cooling (UOC), and (4) unprotected loss of flow (ULOF) . The main criteria for selecting these transients were the availability of data sets from the other tools, in addition to the feasibility and level of complexity required to model the transient in TRACE-PARCS.

A major incentive for exploring the use of a system code rather than a CFD code is the potential for dramatically reducing the computational power required. While the presented TRACE-PARCS calculations could be run on a single 2.6 GHz Intel Xeon processor, no considerable benefit was found compared to CFD codes in terms of computational times. Wall clock times spanning several days were common for computing transients lasting about five minutes in simulation time. Potential exists for optimising these simulations, and investigations into acceleration techniques are merited. Proposed measures include reducing the number of neutronic cells, taking advantage of symmetry options in PARCS, further optimising the DNP calculation routine in TRACE, and exploring parallelisation through geometry decomposition.

4.2.1 Unprotected loss of heat sink

A complete loss of heat sink would occur in the MSFR if the intermediate or tertiary circuit were to lose either inventory or pumping power. The latter scenario has been simulated with TRACE-PARCS by reducing the mass flow rate of the secondary system to zero according to an exponential decay with a time constant of 1.0 s. As a result, the secondary side of the heat exchanger will contain stagnant salt at the end of the transient. This differs from the implementation in TRACE-PK and COMSOL, where the heat transfer coefficient between the primary and secondary sides of the heat exchanger itself has been reduced to zero following a similar exponential decay. The results for all three codes are reported in figures 4.10 and 4.11, where graphs depicting the evolution of power, average core temperature, and the difference between the inlet and outlet temperatures are shown.

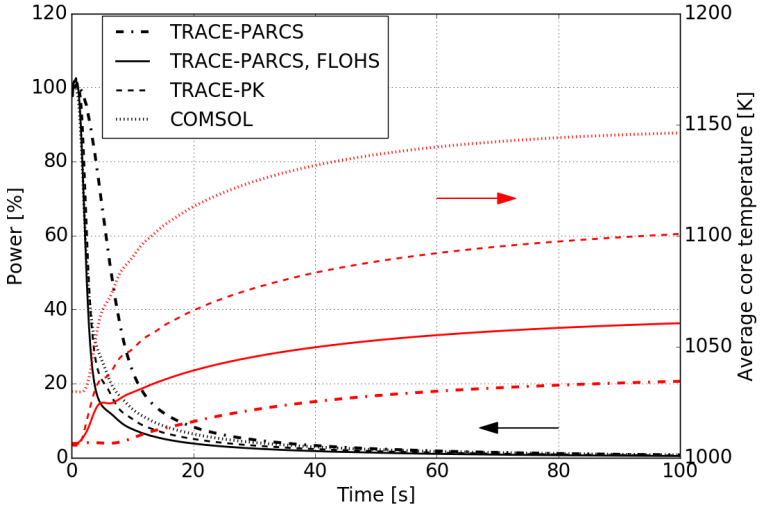

Figure 4.10: Power (black) and average core temperature (red) versus time as calculated by TRACE-PARCS, TRACE-PK, and COMSOL for the ULOHS transient. The abbreviation FLOHS stands for "faster loss of heat sink".

All three tools can be seen to agree on the underlying dynamics of the transient. As the ability to discard the generated fission heat is lost, the primary salt rapidly heats up. In turn, the negative

[7] In this context, unprotected means that no safety system actuates.

temperature feedback ensures that power levels are greatly reduced. The average core temperature can be seen to rise uniformly throughout the transient and gradually reach an asymptotic value as the fission chain reaction dies down and a uniform temperature distribution is established. In reality, the primary circuit is not adiabatic outside of the heat exchanger, and heat transfer through the vessel walls and to the blanket salt should be considered in future models.

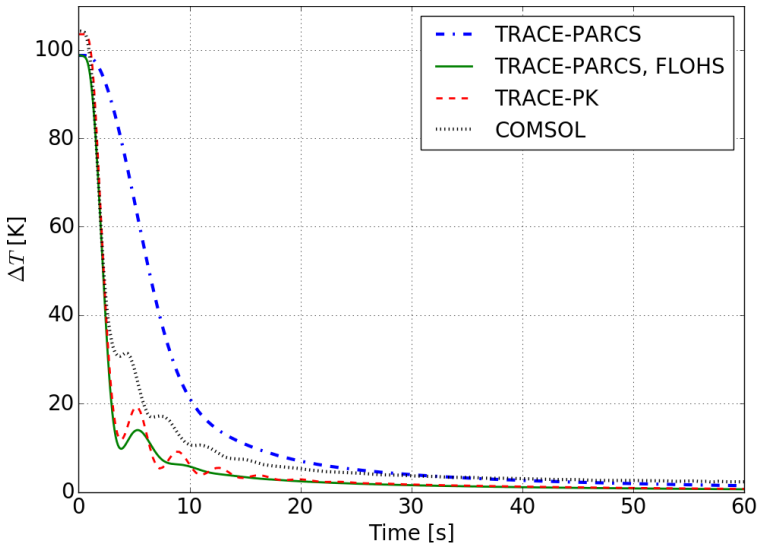

Figure 4.11: $\Delta T = T_{\text{core,outlet}} - T_{\text{core,inlet}}$ as a function of time as calculated by TRACE-PARCS. TRACE-PK, and COMSOL for the ULOHS transient. The abbreviation FLOHS stands for "faster loss of heat sink".

The TRACE-PARCS response is observed to be slower than for the two other tools. This is because the primary circuit is able to transfer heat to the intermediate salt for a longer time on account of the more realistic heat exchanger modelling. As a way to confirm this, an additional simulation, denoted "faster loss of heat sink", or FLOHS, has been performed in which the heat exchange is instantly reduced to zero by equalling the temperature on the secondary side of the heat exchanger with the temperature on the primary side. Both power and ΔT are then reduced at least as rapidly as the other predictions.

Interestingly, the oscillatory behaviour of ΔT, seemingly correlated with the transit time, can be seen to disappear in the nominal TRACE-PARCS simulation. This illustrates that the modelling of temperature distributions along both sides of the heat exchanger has an averaging and smoothing effect on localised temperature variations such as hot or cold slugs of salt. In comparison, TRACE-PK and COMSOL both rely on constant secondary side temperatures, which hardens the response. Clearly, care must be taken with simplified boundary condition approaches for such strongly coupled systems. Otherwise, as has been demonstrated, artificial dynamic behaviour can be introduced, or failed to be captured.

The final average core temperature also varies between the codes. COMSOL predicts the higher value since the larger recirculation zone stores more thermal energy at the beginning of the transient than for the three TRACE implementations. The lower value is predicted by the nominal TRACE-PARCS simulation where more energy has been exchanged to the intermediate circuit over the course of the transient. Finally, TRACE-PK predicts a higher value than the FLOHS simulation because more energy has been deposited in the salt (equal to the integral under the power curves).

4.2.2 Unprotected pump over-speed

Reactivity control of the MSFR is to be accomplished primarily by variations of the primary mass flow rate, and no control rods are included in the current design. The 16 primary pumps will be essential for achieving this, and necessarily feature an intricate control system to finely tune their rotational speeds. A pump over-speed scenario could result from either a system malfunction or operator error, causing an unintended increase of mass flow rate with a resulting positive reactivity insertion. This transient has been simulated in TRACE-PARCS, TRACE-PK, and COMSOL by increasing the primary mass flow rate by 50 % according to the expression $\dot{m}(t) = \dot{m}_0[1 + 0.5 \cdot (1 - e^{-t/\tau})]$, with $\tau = 5$ s and $\dot{m}_0$ representing the mass flow rate at the beginning of the transient ($t = 0$). The results are given in figures 4.12 - 4.14 in the form of mass flow rate, power, and ΔT as calculated by the three different tools.

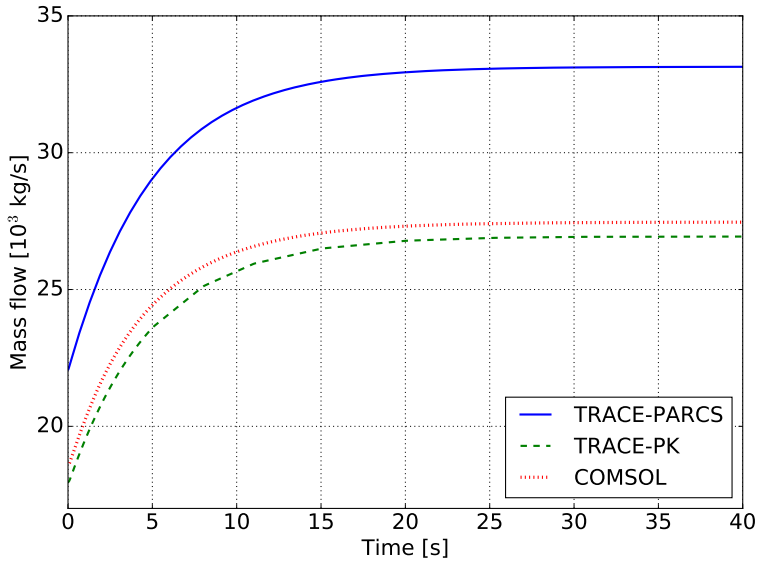

Figure 4.12: Mass flow rates are increased by 50 % in order to simulate the UOS transient.

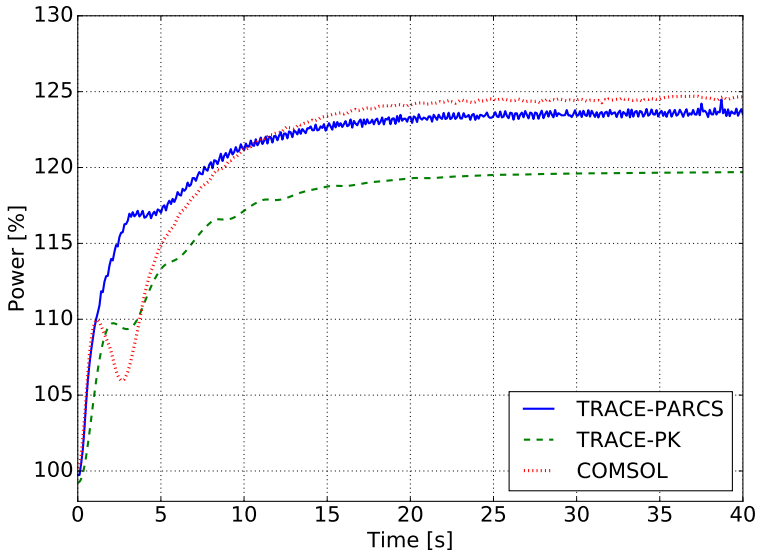

Figure 4.13: Power versus time as calculated by TRACE-PARCS, TRACE-PK, and COMSOL for the UOS transient.

Despite the difference in initial mass flow rate caused by the different specific heat capacities used,

the overall transient behaviour predicted by the three codes is again in agreement. As the pump speeds up, on one hand β_{eff} decreases, while on the other cold salt reaches further into the core before being heated up. The dominant contribution comes from the latter effect, and the positive reactivity introduced is rapidly translated into an increase of power. With the increase in mass flow rate, a smaller enthalpy difference between inlet and outlet is required to carry away the produced power, and so ΔT decreases. Not shown in the plots are the average core temperatures, which stay almost constant throughout the transient. Specifically, the variations are -2.9 K, -2.5 K, and +2.3 K for TRACE-PARCS, TRACE-PK, and COMSOL, respectively, between the beginning and end of the simulation.

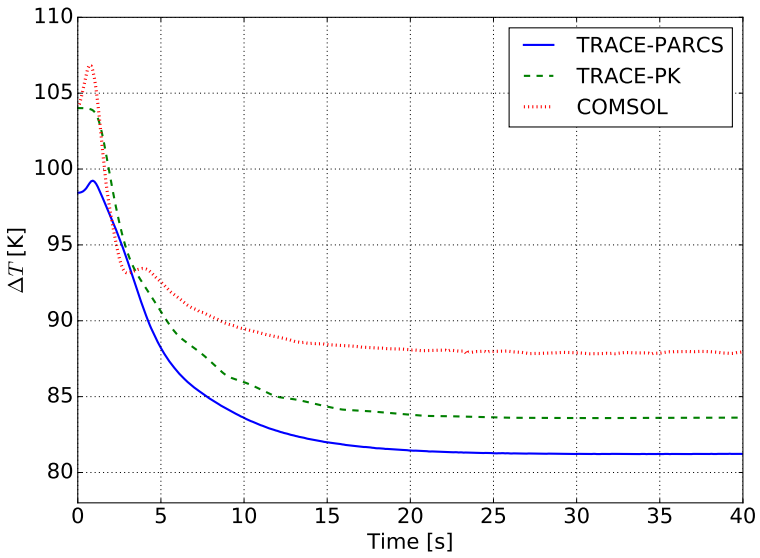

Figure 4.14: $\Delta T = T_{\text{core,outlet}} - T_{\text{core,inlet}}$ as a function of time as calculated by TRACE-PARCS. TRACE-PK, and COMSOL for the UOS transient.

The main difference between the simulations is ΔT. In TRACE-PARCS the asymptotic value is below those of TRACE-PK and COMSOL because the mass flow rate is greater, and so the enthalpy increase in the core is smaller. Since also the magnitude of the mass flow rate increase is greater in the TRACE-PARCS simulation, the difference between ΔT from COMSOL and TRACE-PARCS has increased at the end of the simulation. The TRACE-PK simulation differs in that the asymptotic power level is lower than for the two other codes. According to [Zanetti, 2016], this discrepancy is suspected to be caused by the variations of the β_{eff} incurred by the mass flow rate increase. Lastly, power and ΔT fluctuations related to the simplified heat exchanger implementation in COMSOL and TRACE-PK are again suppressed in the TRACE-PARCS simulation.

4.2.3 Unprotected over-cooling

Regardless of the choice of working fluid in the tertiary turbine circuit of an MSFR plant, be it water or super critical CO_2, it will have to be pressurised. Thus, a possibility will exist for the tertiary circuit to be inadvertently depressurised releasing large quantities of thermal energy in an uncontrolled fashion. This will, in turn, extract excessive amounts of heat from the intermediate circuit, which will cool the primary circuit. Such over-cooling transient can be simulated by reducing the inlet temperature on the secondary side of the primary heat exchanger by 100 K according to an exponential decay with a time constant of 1 s. This has been performed in TRACE-PARCS, while in TRACE-PK and COMSOL the imposed temperature on the secondary side of the heat exchanger was lowered similarly. The results are presented in figures 4.15 - 4.17.

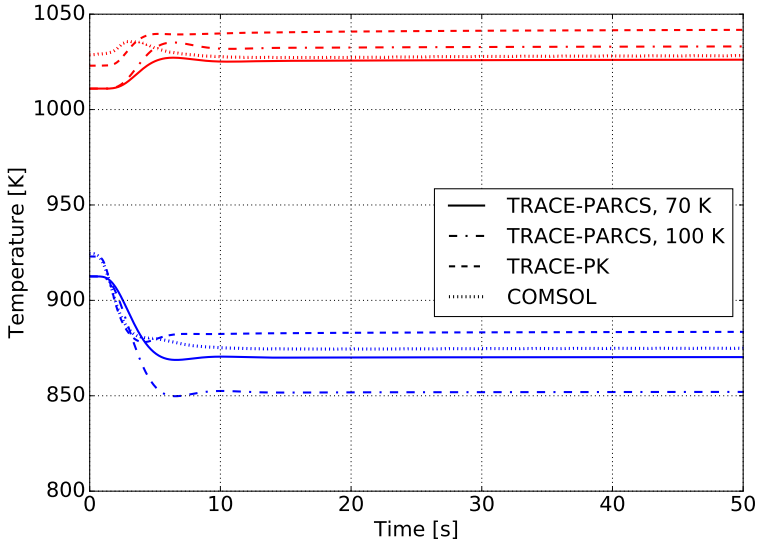

Figure 4.15: Inlet (blue, bottom) and outlet temperatures (red, top) as a function of time as calculated by TRACE-PARCS, TRACE-PK, and COMSOL for the UOC transient. 70 K denotes an additional simulation in which the temperature at the inlet of the heat exchanger was lowered by 70 K instead of 100 K.

Like the UOS transient, the evolution of the UOC transient is driven by the introduction of cold salt into the reactor core as the core inlet temperature is decreased. In response, the neutronic power increases until a new equilibrium between heat generation and removal is established. In figure 4.16, both TRACE codes show the initial decrease in average core temperature (albeit damped in the TRACE-PARCS simulations because of the more realistic heat exchanger), followed by an increase until the reactor stabilises at the new equilibrium power level. For COMSOL, the core temperature evolution is decreasing. Thus, it appears as if the decreased inlet temperature interferes with and reduces the size of the hot recirculation zone. This dynamic behaviour is not reproduced by either TRACE code.

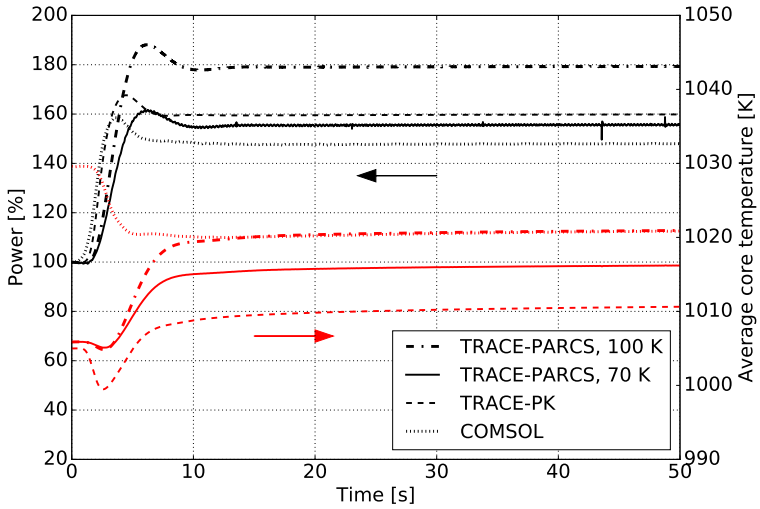

Figure 4.16: Power (black) and average core temperature (red) versus time as calculated by TRACE-PARCS, TRACE-PK, and COMSOL for the UOC transient. 70 K denotes an additional simulation in which the temperature at the inlet of the heat exchanger was lowered by 70 K instead of 100 K.

As can be seen in figure 4.15, the decrease in core inlet temperature is greater in the TRACE-PARCS simulation than for the two other codes. In fact, an inlet temperature of 850 K is only

about 10 K above the melting point of the salt, and should be avoided. Evidently, the TRACE-PARCS model experiences a greater increase in heat transfer following the decrease in secondary side inlet temperature than the other models[8]. Consequently, the power increase reported in figure 4.16 is greater for TRACE-PARCS, as well as the increase in ΔT in figure 4.17.

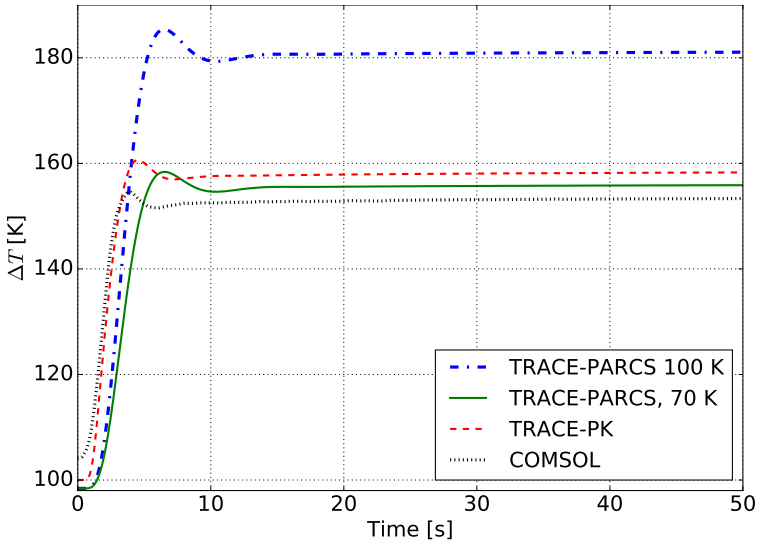

Figure 4.17: $\Delta T = T_{\text{core,outlet}} - T_{\text{core,inlet}}$ as a function of time as calculated by TRACE-PARCS, TRACE-PK, and COMSOL for the UOC transient. 70 K denotes an additional simulation in which the temperature at the inlet of the heat exchanger was lowered by 70 K instead of 100 K.

An additional simulation has been performed in which the temperature at the inlet of the heat exchanger has been decreased by 70 K instead of 100 K. As can be seen in figure 4.15, the core inlet temperature then corresponds better with the results from COMSOL and PARCS-PK. Consequently, also power and ΔT display improved agreement. Some discrepancy persists, such as the difference in average core temperature between the TRACE codes. The initial depression in TRACE-PK indicates a similar disturbance of the recirculation zone as was the case for COMSOL, which is not present in TRACE-PARCS.

4.2.4 Unprotected loss of flow

An unprotected loss of flow transient would occur in the MSFR if one or several primary pumps were to malfunction and end forced circulation in the associated recirculation loop. The bounding transient is the case in which all the pumps stop functioning simultaneously. This has been simulated in TRACE-PARCS, TRACE-PK, and COMSOL by coasting down the primary pumps according to an exponential decay with a time constant of 8 s. Figures 4.18 - 4.20 show the evolution of mass flow rate, power, average core temperature, and ΔT throughout this transient.

[8]The reason for this is related to the differences in heat exchanger modelling and elevated mass flow in the TRACE-PARCS model, which combine non-trivially to produce the observed behaviour

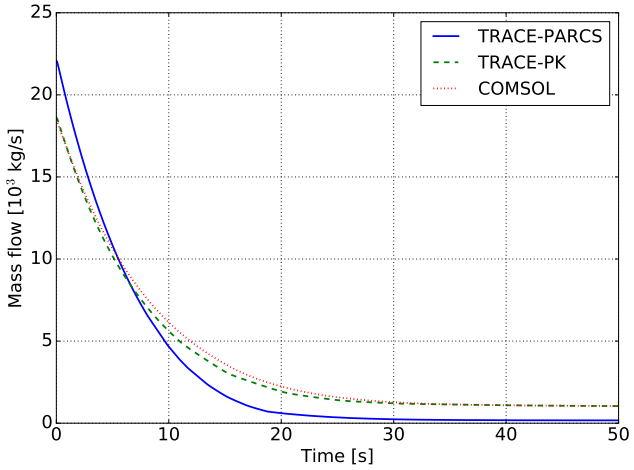

Figure 4.18: Mass flow rate as a function of time as calculated by TRACE-PARCS, TRACE-PK, and COMSOL for the ULOF transient. While natural circulation is established in the COMSOL and TRACE-PK simulations, TRACE-PARCS predicts almost stagnation of the fuel salt.

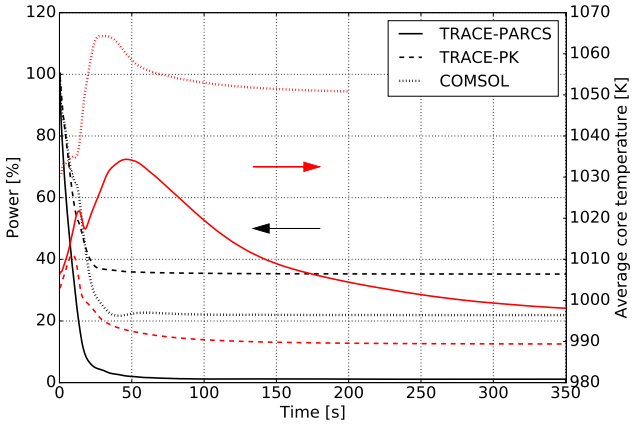

Figure 4.19: Power (black) and average core temperature (red) as a function of time as calculated by TRACE-PARCS, TRACE-PK, and COMSOL for the ULOF transient. The average core temperature evolution for the COMSOL simulation was only calculated until 200 s.

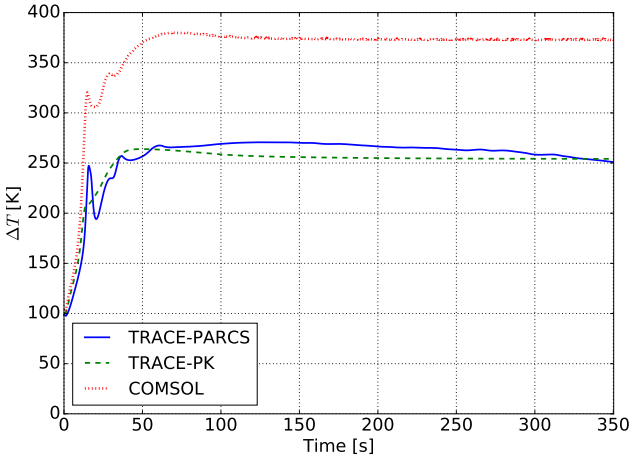

Figure 4.20: $\Delta T = T_{\text{core,outlet}} - T_{\text{core,inlet}}$ as a function of time as calculated by TRACE-PARCS, TRACE-PK, and COMSOL for the ULOF transient.

For this transient, the three codes do not agree on the general dynamics. Whereas natural circula-

tion is established in TRACE-PK and COMSOL, TRACE-PARCS predicts near-stagnation of the fuel salt. As a consequence, the reactor experiences both degraded heat removal and an increased β_{eff} that work together to increase the temperature until the neutron chain reaction is effectively stopped by temperature feedbacks. However, since the secondary side continues to extract heat, the average core temperature begins to decline. Furthermore, in the now nearly stagnant core, hot salt floats to the top and cold salt sinks to the bottom, creating a large temperature gradient that maintains a high ΔT. As more thermal energy is extracted in the heat exchanger, the cold region at the bottom creeps upwards and the core gradually approaches a uniform temperature distribution.

The absence of natural circulation in TRACE-PARCS is a result of having the heat exchanger placed below the pump. Placing the heat sink, i.e., the heat exchanger, at an elevated position compared to the heat source, i.e., the core, benefits natural circulation, and has been done in the two other models. As a result, TRACE-PK and COMSOL calculate a mass flow rate about ten time greater than TRACE-PARCS at the new equilibrium conditions. In an attempt to improve the comparison, TRACE-PARCS simulations have been performed with the heat exchanger on top of the pump. However, as the length of the heat exchanger made it impossible to place it as high as in the other models, only modest improvements were observed and considerate discrepancies persisted.

Evidently, also TRACE-PK and COMSOL compute quite different solutions. In fact, in a comparison between COMSOL and another CFD-based tool from TU Delft, significant discrepancies between the computed behaviours in the ULOF transient are also reported [Fiorina, 2013]. This indicates that this transient is particularly sensitive to the modelling of components such as heat exchangers, pumps, as well as treatment of friction. Adding to the complexity, natural circulation of fluids with internal heat generation from the distributed decay heat constitutes a largely unexplored field that is currently under investigation [Cammi et al., 2016].

Finally, it is noted that current plans for decay heat removal (DHR) relies on dumping the salt to the dump tanks where the heat can be more easily removed. Despite this, several incentives for studying the natural circulation phenomenon exist. First, an increased reliance on natural circulation for DHR could improve plant economics by avoiding the draining, freezing and eventual thawing and reintroduction of the salt from the drain tanks. Second, natural circulation would have to be relied on in case of malfunction in the drainage system. Third, considerable time might pass while the salt is in the process of draining. Natural circulation would provide additional heat removal during this time interval.

5 Conclusions and outlook

This thesis has reported the application of the coupled TRACE-PARCS multi-physics code to transient analyses of the MSFR. The main goal has been to assess the ability of this tool to predict dynamic behaviour of the MSFR through comparison with alternative code systems. A secondary goal has been to display and characterise distinguishing features of MSRs based on the steady-state and transient simulations performed.

In order to assemble the coupled tool, a simplified, axially-symmetric benchmark model of the MSFR was separately implemented in the codes TRACE, PARCS, and Serpent. The purpose of the Serpent model was to generate spatially homogenised, multi-group, macroscopic cross sections that allowed PARCS to capture the strong temperature feedback effects exhibited by the MSFR. To advise the modelling of the breeding blanket, Monte Carlo simulations were performed with MCNP to investigate power deposition during steady-state. The blanket was found to have negligible influence on the primary circuit, and was thus neglected in the TRACE and PARCS models. However, under transient conditions a stronger influence is likely and warrants further investigation.

Steady-state simulations were performed with the three codes in order to initialise transient calculations and to explore the MSFR phenomenology. Neutron flux distribution and spectrum, temperature feedback coefficients, primary circuit temperature, pressure, velocity, and DNP distributions, the effective delayed neutron fraction, and transit time have been investigated and discussed.

Comparisons of the thermal-hydraulic steady-state solution were made with a CFD solver based on COMSOL. Although TRACE proved unable to reproduce the level of detail of COMSOL, main features were found to be consistent after calibration against the COMSOL solution. An important source of discrepancy was the difference in specific heat capacity values used in the two codes. TRACE used a lower value, and thus required a higher mass flow rate to maintain the same temperature rise over the core. Similarly, the neutronic steady-state solution calculated by PARCS was found to correlate well with Serpent after an initial calibration of the albedo condition. Discrepancies on the order of 1-2 % in temperature coefficients are reported. The need for higher-accuracy solutions to calibrate the steady-state models should be emphasised, as this requirement will also apply to the coupled tool.

Four transients were simulated with TRACE-PARCS and compared with solutions from the CFD-tool COMSOL (coupled with a spatial diffusion solver) and TRACE-PK (TRACE together with a simplified point kinetics routine). The three tools were found to generally agree on transient dynamics. However, direct comparison was often complicated due to differences in modelling. For instance, the heat exchangers were implemented in a more realistic manner in TRACE-PARCS. Where more direct comparisons were facilitated, reasonable agreement was found. As such, the observed discrepancies are in large parts due to differences in modelling. Of the discrepancies that could not be traced to modelling choices (e.g. the evolution of average core temperature), many are related to differences in the underlying equations solved by the codes and the resolution of the computational meshes. Based on these observations and insights, it is concluded that the TRACE-PARCS coupled tool, to a reasonable extent, is able to reproduce the main features of dynamic MSFR behaviour as predicted by the other multi-physics tools.

A particularly interesting discrepancy between TRACE-PARCS and the two other tools was the existence of power and temperature oscillations with characteristic times similar to the transit time. While COMSOL and TRACE-PK predicted such fluctuations in the UOS and ULOHS transients, TRACE-PARCS showed a much smoother behaviour. It has been shown that this behavioural difference stems from the explicit modelling of a secondary circuit in TRACE-PARCS, whereas COMSOL and TRACE-PK impose a constant secondary side temperature. This highlights the importance of imposed boundary conditions on strongly coupled systems such as the MSFR.

In general, TRACE-PARCS seems to agree well with TRACE-PK. This indicates that spatial kinetics are not required to model the transients investigated herein, but that point kinetics are sufficient. Since point kinetics calculations are also faster to execute, they represent the superior alternative when little to no asymmetry is expected. Conversely, for asymmetric transients such as single pump failure, spatial kinetics tools are expected to yield more accurate solutions.

One notable exception to the general agreement between the three tools was the ULOF transient. It exhibits strong dependence on modelling choices related to pumps, heat exchangers, as well as treatment of friction, which makes it particularly complicated to simulate. Furthermore, it considers natural circulation of internally heated fluids, for which systematic investigation has only recently begun [Cammi et al., 2016].

Ultimately, TRACE-PARCS has been found to represent a viable tool for calculating transient behaviour of the MSFR when computational resources are scarce or the considered model is large. That being said, while only a single processor was used to run transients on, computational times were prohibitively long, commonly several days. Attempts at optimising the MSFR model implementations as well as the TRACE-PARCS tool are therefore merited. The availability of built-in component models in TRACE facilitated realistic modelling of heat exchangers and pumps, while the comprehensive control logic system simplified the simulation of transients. In sum, TRACE-PARCS represents a flexible and powerful multi-physics code that can be easily extended to investigate additional transients and more extensive MSFR plant systems.

Continued research into TRACE-PARCS and related topics could progress in a number of different directions. First and foremost, efforts should be made at improving the computational efficiency to accelerate calculations. Suggestions include model order reduction, employing symmetry options in PARCS, further optimising the DNP solution routine in TRACE, and enabling parallelisation through domain decomposition. With improved run times, an extension to full three-dimensional models is straightforward and would permit investigation of asymmetric transients so as to further assess the influence of the spatial kinetics solution.

Only the primary and a simplified secondary circuit were considered in this project. However, as TRACE is equipped with two-phase flow equations, the modelling of entire MSFR plants including turbine circuits with liquid water and steam is readily attainable. Moreover, two-phase fluid capabilities can be used to model gas bubbles in the molten salt. Thus, the effects of fission gas formation and tritium bubble inclusion in the primary salt can be studied, or the helium bubbling technique that has been proposed to extract fission products from the MSFR [Journée, 2014].

Lastly, an additional area to explore is the coupling of a system code such as TRACE with a high-accuracy CFD code. In such an arrangement, thermal-hydraulic behaviour within and out-of-core would be calculated by the CFD and system code, respectively. Explicit coupling is accomplished by data transfer at the boundaries between the two models. Thus, computational requirements are kept manageable by only invoking the CFD solver in a restricted region of space. Furthermore, for the specific case of TRACE, such symbiosis would overcome the restriction of rectangular or cylindrical core shapes that currently limit the applicability of TRACE to more recent MSFR design iterations. Some investigations into this area exist [Bertolotto, 2011; Zanetti, 2016], although more remain to be learned.

Bibliography

[Ariu, 2014] Ariu, V. (2014). Heat exchanger analysis for innovative molten salt fast reactor. Master's thesis, Eidgenössische Technische Hochschule Zürich (ETHZ) and École polytechnique fédérale de Lausanne (EPFL).

[Aufiero, 2014] Aufiero, M. (2014). *Development of advanced simulation tools for circulating-fuel nuclear reactors*. PhD thesis, Politecni di Milano, Department of Energy.

[Aufiero et al., 2014] Aufiero, M., Cammi, A., Geoffroy, O., Losa, M., Luzzi, L., Ricotti, M. E., and Rouch, H. (2014). Development of an OpenFOAM model for the Molten Salt Fast Reactor transient analysis. *Chemical Engineering Science*, 111:390–401.

[Auger et al., 2008] Auger, T., Barreau, G., Chevalier, J.-P., Doligez, X., Delpech, S., Flocard, H., Haas, B., Heuer, D., and Merle-Lucotte, E. (2008). The CNRS Research Program on the Thorium cycle and the Molten Salt Reactors. Technical report, Centre National de la Recherche Scientifique.

[Beneš and Konigs, 2012a] Beneš, O. and Konigs, R. J. M. (2012a). Molten Salt Reactor Fuel and Coolant. In Konigs, R. J. M., editor, *Comprehensive Nuclear Materials*, chapter 3.13. Elsevier Ltd.

[Beneš and Konigs, 2012b] Beneš, O. and Konigs, R. J. M. (2012b). Thermodynamic Calculations of Molten-Salt Reactor Fuel Systems. In Konigs, R. J. M., editor, *Comprehensive Nuclear Materials*, chapter 4. Elsevier Ltd.

[Bertolotto, 2011] Bertolotto, D. (2011). *Coupling a System Code with Computational Fluid Dynamics for the Simulation of Complex Coolant Reactivity Effects*. PhD thesis, École polytechnique fédérale de Lausanne (EPFL).

[Brovchenko, 2013] Brovchenko, M. (2013). *Études préliminaires de sûreté du réacteur à sels fondus MSFR*. PhD thesis, Laboratoire de Physique Subatomique et de Cosmologie de Grenoble, Université Grenoble Alpes.

[Cammi et al., 2016] Cammi, A., Cauzzi, M., Luzzi, L., and Pini, A. (2016). Dynasty: an experimental loop for the study of natural circulation with internally heated fluids. In *Conference: 12th International Conference on Heat Transfer, Fluid Mechanics and Thermodynamics (HEFAT 2016)*, Malaga, Spain.

[Chadwick et al., 2011] Chadwick, M. B., Herman, M., Obložinský, P., Dunn, M. E., Danon, Y., Kahler, A. C., Smith, D. L., Pritychenko, B., Arbanas, G., Arcilla, R., Brewer, R., Brown, D. A., Capote, R., Carlson, A. D., Cho, Y. S., Derrien, H., Guber, K., Hale, G. M., Hoblit, S., Holloway, S., Johnson, T. D., Kawano, T., Kiedrowski, B. C., Kim, H., Kunieda, S., Larson, N. M., Leal, L., Lestone, J. P., Little, R. C., McCutchan, E. A., MacFarlane, R. E., MacInnes, M., Mattoon, C. M., McKnight, R. D., Mughabghab, S. F., Nobre, G. P. A., Palmiotti, G., Palumbo, A., Pigni, M. T., Pronyaev, V. G., Sayer, R. O., Sonzogni, A. A., Summers, N. C., Talou, P., Thompson, I. J., Trkov, A., Vogt, R. L., van der Marck, S. C., Wallner, A., White, M. C., Wiarda, D., and Young, P. G. (2011). ENDF/B-VII.1 nuclear data for science and technology: Cross sections, covariances, fission product yields and decay data.

[Cherubini et al., 2011] Cherubini, F., Peters, G., Berntsen, T., Strømman, A. H., and Hertwich, E. (2011). CO2 emissions from biomass combustion for bioenergy: atmospheric decay and contribution to global warming. *GBC Bioenergy*, 3.

[CNSC, 2015] CNSC (2015). Update on Regulatory Vendor Design Review of Advanced Reactor Designs in Canada. Presentation to the IAEA by R. P. Rulko.

[COMSOL, 2012] COMSOL (2012). COMSOL Multiphysics User's Guide. COMSOL, Inc., version 4.3a.

[Doligez, 2010] Doligez, X. (2010). *Influence du retraitement physico-chimique du sel combustible sur le comportement du MSFR et sur le dimensionnement de son unité de retraitement*. PhD thesis, Institut National Polytechnique de Grenoble (INPG).

[Downar et al., 2009] Downar, T., Xu, Y., and Seker, V. (2009). Purdue Advanced Reactor Core Simulator (PARCS) v.3 Theory Manual.

[Fiorina, 2013] Fiorina, C. (2013). *The Molten Salt Fast Reactor as a Fast-Spectrum Candidate for Thorium Implementation*. PhD thesis, Politecnico di Milano, Department of Energy.

[Fiorina et al., 2013] Fiorina, C., Aufiero, M., Cammi, A., Franceschini, F., Křepel, J., Luzzi, L., Mikityuk, K., and Ricotti, M. E. (2013). Investigation of the MSFR core physics and fuel cycle options. *Progress in Nuclear Energy*, 68.

[Forsberg et al., 2003] Forsberg, C. W., Peterson, P. F., and Pickard, P. S. (2003). Molten-Salt-Cooled Advanced High-Temperature Reactor for Production of Hydrogen and Electricity. *ANS Nuclear Technology*, 144:289–302.

[Ghasabyan, 2013] Ghasabyan, L. K. (2013). Use of Serpent Monte-Carlo code for development of 3D full-core models of Gen-IV fast-spectrum reactors and preparation of group constants for transient analyses with PARCS/TRACE coupled system. Master's thesis, Royal Institute of Technology, KTH.

[GIF, 2002] GIF (2002). A Technology Roadmap for Generation IV Nuclear Energy Systems. Issued by the U.S. DOE Nuclear Energy Research Advisory Committee and the Generation IV International Forum.

[Haubenreich and Engel, 1970] Haubenreich, P. N. and Engel, J. R. (1970). Experience with the Molten-Salt Reactor Experiment. *Nuclear applications and technology*, 8.

[Haynes International, 2015] Haynes International (2015). HASTELLOY®N alloy. Product brochure available from haynesintl.com [PDF].

[IEA, 2015a] IEA (2015a). Key World Energy Statistics.

[IEA, 2015b] IEA (2015b). *World Energy Outlook*. OECD/IEA. ISBN: 978-92-64-24365-1.

[Johnson, 2009] Johnson, E. (2009). Goodbye to carbon neutral: Getting biomass footprints right. *Environmental Impact Assessment Review*, 29.

[Journée, 2014] Journée, D. (2014). Helium bubbling in a Molten Salt Fast Reactor. Master's thesis, Delft University of Technology, Faculty of Applied Physics.

[Kakodkar and Degweker, 2013] Kakodkar, A. and Degweker, S. B. (2013). Towards Sustainable, Secure, and Safe Energy Future: Leveraging Opportunities with Thorium. In *Proceedings of the ThEC13 Conference*, Geneva, Switzerland.

[Kedl, 1972] Kedl, R. J. (1972). The migration of a class of fission products (noble metals) in the molten-salt reactor experiment. Technical report, ORNL. ORNL-TM-3884.

[Kim, 2015] Kim, H.-M. (2015). Static and transient analysis of Molten Salt Reactor Experiment using SERPENT-2/TRACE/PARCS codes. Master's thesis, Eidgenössische Technische Hochschule Zürich (ETHZ) and École polytechnique fédérale de Lausanne (EPFL).

[Leppänen, 2013] Leppänen, J. (2013). Serpent - a Continuous-energy Monte Carlo Reacter Physics Burnup Calculation Code, User's Manual. VTT Technical Research Centre of Finland. Note: Serpent-2.1.26 has been used throughout this work.

[Leppänen et al., 2014] Leppänen, J., Aufiero, M., Fridman, E., Rachamin, R., and van der Marck, S. (2014). Calculation of effective point kinetics parameters in the Serpent 2 Monte Carlo code. *Annals of Nuclear Energy*, 65:272–279.

[Li et al., 2014] Li, R., Wang, S., Rineiski, A., Zhang, D., and Merle-Lucotte, E. (2014). Transient analyses for a molten salt fast reactor with optimized core geometry. *Nuclear Engineering and Design*.

[MacPherson, 1985] MacPherson, H. G. (1985). The Molten Salt Reactor Adventure. *Nucler Science and Engineering*, 90.

[Mathers and Hesketh, 2013] Mathers, D. and Hesketh, K. (2013). A View on the Thorium Fuel Cycle. In *Proceedings of the ThEC13 Conference*, Geneva, Switzerland.

[Mathieu et al., 2006] Mathieu, L., Heuer, D., Brissot, R., Brun, C. L., Liatard, E., Loiseaux, J.-M., Méplan, O., Merle-Lucotte, E., Nuttin, A., and Wilson, J. (2006). The Thorium Molten Salt Reactor: Moving On from the MSBR. *Progress in Nuclear Energy*, 48.

[Mattioda et al., 2000] Mattioda, F., Ravetto, P., and Ritter, G. (2000). Effective delayed neutron fraction for fluid-fuel systems. *Annals of Nuclear Energy*, 27:1523–1532.

[Merle-Lucotte et al., 2011] Merle-Lucotte, E., Heuer, D., Allibert, M., Brovchenko, M., Capellan, N., and Ghetta, V. (2011). Launching the Thorium Fuel Cycle with the Molten Salt Fast Reactor. In *Proceedings of the International Congress on Advances in Nuclear Power Plants (ICAPP) 2011*, Nice, France.

[Merle-Lucotte et al., 2008] Merle-Lucotte, E., Heuer, D., Allibert, M., Doligez, X., Ghetta, V., and Brun, C. L. (2008). Optimization and simplification of the concept of non-moderated Thorium Molten Salt Reactor. In *Proceedings of the International Conference on the Physics of Reactors (PHYSOR) 2008*, Interlaken, Switzerland.

[Mikityuk et al., 2005] Mikityuk, K., Pelloni, S., Coddington, P., Bubelis, E., and Chawla, R. (2005). FAST: An advanced code system for fast reactor transient analysis. *Annals of Nuclear Energy*, 32.

[Nagy et al., 2010] Nagy, K., Kloosterman, J. L., Lathouwers, D., and van der Hagen, T. H. J. J. (2010). New breeding gain definitions and their application to the optimization of a molten salt reactor design. *Annals of Nuclear Energy*, 38.

[NEA, 2015] NEA, O. (2015). Introduction of Thorium in the Nuclear Fuel Cycle - Short- to long-term considerations . NEA no. 7228.

[NRC, 2007] NRC (2007). TRACE v.5 User's Manual.

[NRC, 2012] NRC (2012). Report to Congress: Advanced Reactor Licensing.

[Patankar, 1980] Patankar, S. V. (1980). *Numerical Heat Transfer and Fluid Flow*. Hemisphere Publishing Corporation.

[Pelowitz et al., 2014] Pelowitz, D. B., Fallgren, A. J., and (Eds.), G. E. M. (2014). MCNP6 User's Manual.

[Penny, 2010] Penny, S. L. (2010). A Study of the Advantages of Thorium Reactors for Nuclear Power. Master's thesis, Faculty of Engineering and Physical Sciences, University of Surrey.

[Pioro, 2016] Pioro, I., editor (2016). *Handbook of Generation IV Nuclear Reactors*. Woodhead Publishing. ISBN: 9780081001493.

[Pope and Mousseau, 2009] Pope, M. A. and Mousseau, V. A. (2009). Accuracy and efficiency of a coupled neutronics and thermal hydraulics model. *Nuclear Engineering and Technology*, 41.

[Rangel and Leveque, 2015] Rangel, L. E. and Leveque, F. (2015). Revisiting the Cost Escalation Curse of Nuclear Power: New Lessons from the French Experience. *Economics of Energy & Environmental Policy*, 4.

[Rimpault et al., 2002] Rimpault, G., Plisson, D., Tommasi, J., Jacqmin, R., Rieunier, J.-M., Verrier, D., and Biron, D. (2002). The ERANOS code and data system for fast reactor neutronic analyses. In *Proceedings of the International Conference on the Physics of Reactors (PHYSOR)*, Seoul, Korea.

[Rosenthal, 2009] Rosenthal, M. W. (2009). An Account of Oak Ridge National Laboratory's Thirteen Nuclear Reactors. ORNL/TM-2009/181.

[Rouch et al., 2014] Rouch, H., Geoffroy, O., Rubiolo, P., Laureau, A., Brovchenko, M., Merle-Lucotte, E., and Heuer, D. (2014). Preliminary Thermal-hydraulic Core Design of the Molten Salt Fast Reactor (MSFR). *Annals of Nuclear Energy*.

[Sabharwall et al., 2011] Sabharwall, P., Kim, E. S., McKellar, M., and Anderson, N. (2011). Process Heat Exchanger Options for Fluoride Salt High Temperature Reactor. Technical report, Idaho National Laboratory. Prepared for the U.S. Department of Energy.

[Samuel, 2009] Samuel, D. (2009). Molten salt coolants for high temperature reactors - a literature summary of key R&D activities and challenges. Technical report, IAEA INPRO. Internship report for the INPRO COOL collaborative project.

[Santamarina et al., 2009] Santamarina, A., Bernard, D., Blaise, P., Coste, M., Courcelle, A., Huynh, T., Jouanne, C., Leconte, P., Litaize, O., Mengelle, S., Noguère, G., Ruggiéri, J.-M., Sérot, O., Tommasi, J., Vaglio, C., and Vidal, J.-F. (2009). The JEFF-3.1.1 Nuclear Data Library. Technical report, OECD NEA. ISBN 978-92-64-99074-6.

[Serp et al., 2014] Serp, J., Allibert, M., Beneš, O., Delpech, S., Feynberg, O., Ghetta, V., Heuer, D., Holcomb, D., Ignatiev, V., Kloosterman, J. L., Luzzi, L., Merle-Lucotte, E., Uhlíř, J., Yoshioka, R., and Zhimin, D. (2014). The molten salt reactor (MSR) in generation IV: Overview and perspectives. *Progress in Nuclear Energy*, 77.

[Sokolov et al., 2005] Sokolov, F., Fukuda, K., and Nawada, H. P. (2005). Thorium fuel cycle — Potential benefits and challenges. Technical report, IAEA.

[van der Linden, 2012] van der Linden, E. (2012). Coupled neutronics and computational fluid dynamics for the molten salt fast reactor. Master's thesis, Delft University of Technology, Faculty of Applied Physics.

[Waltar et al., 2012] Waltar, A. W., Todd, D. R., and Tsvetkov, P. V. (2012). *Fast Spectrum Reactors*. Springer Science+Business Media, LLC. ISBN 978-1-4419-9571-1.

[X-5 Monte Carlo Team, 2003] X-5 Monte Carlo Team (2003). MCNP - A General Monte Carlo N-Particle Transport Code, Version 5. Volume I: Overview and Theory. LA-UR-03-1987, Los Alamos National Laboratory, Los Alamos, N.M.

[Zanetti, 2016] Zanetti, M. (2016). *Development of new tools for the analysis and simulation of circulating-fuel reactor power plants*. PhD thesis, Politecni di Milano, Department of Energy.

[Zanetti et al., 2015] Zanetti, M., Cammi, A., Luzzi, L., Křepel, J., and Mikityuk, K. (2015). Extension of the FAST code system for the modelling and simulation of MSR dynamics. In *ICAPP 2015: Proceedings of the International Congress on Advances in Nuclear Power Plants*.

List of abbreviations

ARE	Aircraft Reactor Experiment
AU	arbitrary units
CFD	computational fluid dynamics
CMFD	coarse mesh finite difference
DHR	decay heat removal
DNP	delayed neutron precursor
EVOL	Evaluation and Viability Of Liquid fuel fast reactor system
FLiBe	LiF-BeF_2
GIF	Generation IV International Forum
IEA	International Energy Agency
LWR	light water reactor
MSR	molten salt reactor
MSFR	Molten Salt Fast Reactor
MSBR	Molten Salt Breeder Reactor
MSRE	Molten Salt Reactor Experiment
NEA	Nuclear Energy Agency
NRC	US Nuclear Regulatory Commission
ORNL	Oak Ridge National Laboratory
PARCS	Purdue Advanced Reactor Core Simulator
pcm	per cent mille
PSI	Paul Scherrer Institut
PK	point kinetics
TRACE	TRAC/RELAP Advanced Computational Engine
TRACE-PK	the TRACE code extended with DNP and point kinetics capabilities
TU Delft	Delft University of Technology
ULOF	unprotected loss of flow
ULOHS	unprotected loss of heat sink
UOC	unprotected over-cooling
UOS	unprotected pump over-speed
VVER	Vodo-Vodyanoi Energetichesky Reaktor (in English: Water-Water Power Reactor)

Nomenclature

Latin symbols

a	albedo value
c_j	concentration of DNP group j
C_w	wall drag coefficient
cf_{circ}	circulation correction factor
D_m	molecular diffusivity
D_n	neutron diffusion coefficient
e	specific internal energy
f_w	wall friction force (per volume)
g	gravitational constant
J	neutron current
k	turbulent kinetic energy
k_{eff}	neutron multiplication factor
k_w	Churchill correlation friction factor
$\dot{m}$	mass flow rate
n	neutron density
p	pressure
q_f	direct fluid heating
q_w	wall heating
Re	Reynolds number
t	time
T	temperature
$T_{1/2}$	half-life
u	fluid velocity
v	neutron velocity

Greek symbols

α_D	Doppler reactivity coefficient
α_T	overall temperature reactivity coefficient
α_ρ	fuel salt density reactivity coefficient
β_{eff}	effective delayed neutron fraction
β_j	delayed neutron fraction for DNP group j
χ_d	DNP decay neutron yield
χ_p	fission neutron yield
δ	surface roughness
ΔT	Core inlet and outlet temperature difference
ϵ	turbulent dissipation
ν	average number of neutrons per fission
ϕ	neutron flux
ϕ^*	adjoint neutron flux
λ	decay constant
ρ	density
Σ	macroscopic cross section

Boldface indicates vector quantities.

A Coupled code initialisation

Traditionally, the endeavour of obtaining coupled simulations with TRACE and PARCS has been greatly simplified on a code architecture level by incorporating coupled simulation capabilities at an early stage. As a result, an option exists that can simply be enabled or disabled by the user. However, when used in conjunction with the TRACE code extensions and modifications implemented at PSI for the simulation of liquid-fuelled reactors in which DNPs are transported, complexities arise. The aim of this chapter is to document the particular procedure that has been established for obtaining the coupled simulations presented prior to this. As such, it is hoped to augment the results obtained and argumentation followed in the main part of the thesis, as well as provide guidance for anyone interested in performing similar simulations of MSRs by means of the coupled TRACE-PARCS tool.

The established procedure contains three distinct steps; (1) steady-state preparation, (2) input preparation, and (3) transient initialisation. In the following, each of these steps will be discussed separately.

1. Steady-state preparation

Only the thermal-hydraulic steady-state from TRACE is strictly needed in order to begin the coupled calculation, as PARCS solves the time-independent neutron diffusion equation once as soon as the coupled tool is started up. That being said, PARCS must naturally be configured beforehand by running standalone steady-state calculations.

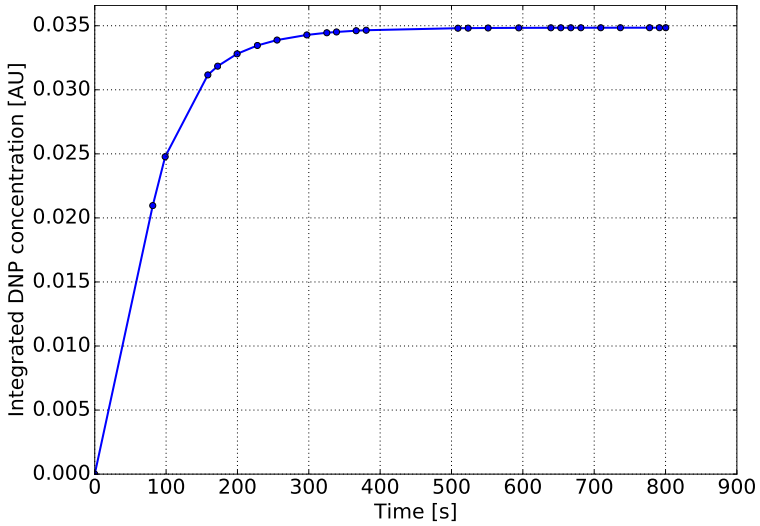

Figure A.1: Spatially integrated DNP concentration as a function of time during steady-state TRACE calculations.

The strategy for obtaining steady-state solutions in TRACE is mainly outlined in chapter 3, with additional details provided in chapter 4. Of particular importance is the assurance that the concentration of DNPs is properly converged. Figure A.1 illustrates the accumulation of DNPs with the DNP parameters used throughout this thesis, from which an approximate convergence time could be determined. In order to be conservative, and because steady-state TRACE simulations were comparatively cheap to perform, 800 s was used throughout.

2. Input preparation

Coupled TRACE-PARCS simulations are initialised from the steady-state TRACE solution by means of something called *restart* calculations. Then, the coupled computation is initialised at velocities, temperatures, and pressures corresponding to a user-specified time step of the steady-state solution which has to be provided as a so-called *trcrst* file. In order to obtain a similar functionality for DNP concentration, a minor code extension was made during this project to output the converged DNP field from the steady-state calculation. By supplying this file under the title *dnprstinput* to the new calculation, the desired functionality is obtained.

Next, a file describing the mapping between thermal-hydraulic cells in TRACE and neutronic cells in PARCS has to be prepared and provided within the same directory. For the preparation of this file, which must be titled *maptab*, a short Fortran routine developed by D. Blanchet was used.

Lastly, a minor modification to the radial mesh used in TRACE must be made in order to obtain the correct power distribution from PARCS. The reason for this is that the total volume of the neutronic cells mapped to one thermal-hydraulic cell (c.f. figure 3.2) differs from the volume of the thermal-hydraulic cell. Since the amount of power deposited in the thermal-hydraulic cell is calculated from the specific power and volume of each PARCS cell, a discrepancy corresponding to the ratio of the volumes is introduced. By correcting the exact position of the TRACE radial mesh delimiters, the two volumes can be aligned and the expected power distribution given to TRACE.

3. Transient initialisation

When the coupled simulation begins, PARCS will be receiving the steady-state DNP concentration as calculated by TRACE. Consequently, as illustrated in figure A.2, the power level is dramatically reduced as DNP transport is suddenly accounted for. In response to this, the salt temperature in the core will decrease to the point where sufficient positive reactivity has been introduced to establish a new equilibrium between power production and removal in the heat exchanger. If no actions are performed to influence this, the new equilibrium settles at a power level of about 80 %. In figure A.2, this occurs after 10 s.

For investigating transients from nominal power, the power level must therefore be returned to 3 GW_{th}. One way of achieving this is to increase the mass flow rate on the secondary side of the heat exchanger. As a result, the salt at the inlet of the core will cool and introduce positive reactivity. In figure A.2, the secondary side mass flow rate has been linearly ramped up over a 30 s interval starting at $t = 15$ s in order to regain nominal power levels. The resulting decrease in inlet temperature is displayed in figure A.3, and amounts to about 25 K. Some time is then allowed for the DNP concentration to recover after the depression suffered from the early drop in power, before the transient is initialised at $t = 80$ s in the figures.

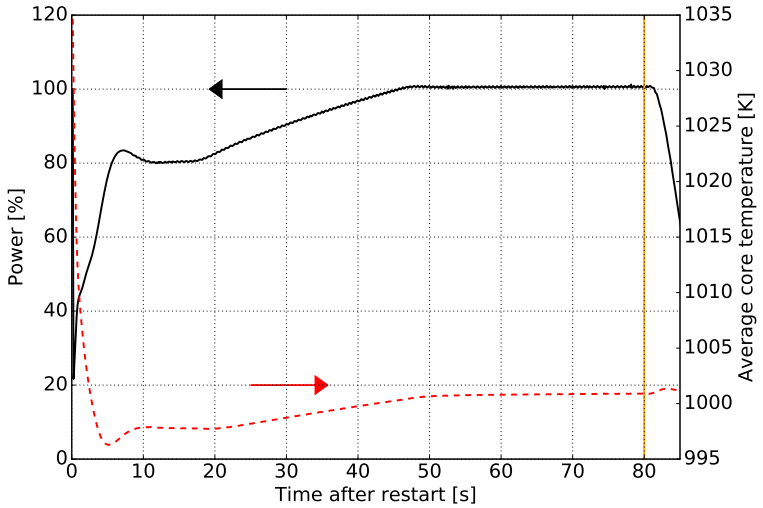

Figure A.2: Power and average core temperature as calculated by TRACE for the time leading up to the beginning of the transient, marked by the vertical, orange line at $t = 80$ s.

Lastly, as evident in figure A.3, ΔT is not exactly equal to 100 K at the beginning of the transient as is the case in the COMSOL and TRACE-PK simulations. To amend this, the primary mass flow rate was reduced from 23800 kg/s to 22150 kg/s so that the outlet temperature increased by about 10 K.

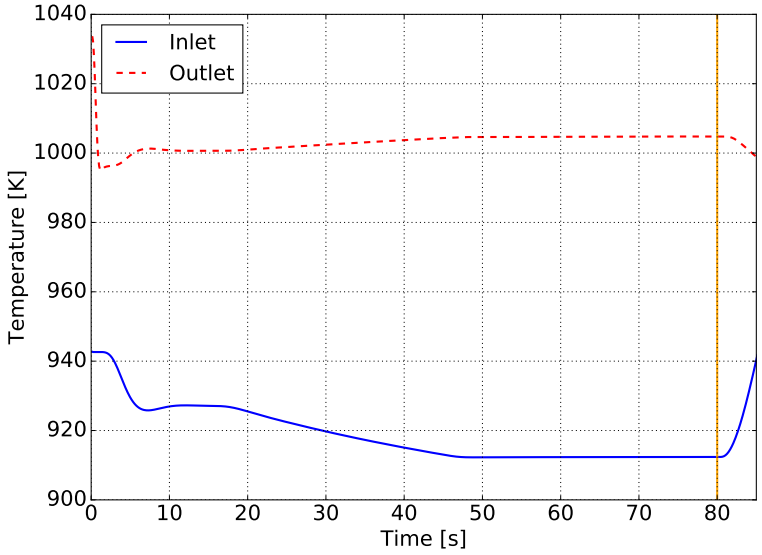

Figure A.3: Core inlet and outlet temperatures as calculated by TRACE for the time leading up to the beginning of the transient, marked by the vertical, orange line at $t = 80$ s.

Acknowledgements

I would like to express my sincerest gratitude to the organisations that funded me while performing the presented work. This includes the GENTLE project that generously awarded me with a grant, as well as KIC InnoEnergy and Statens Lånekasse.

Furthermore, I would like to thank the Paul Scherrer Institut for kindly agreeing to host me for the duration of my master thesis project. Particular mention goes to Konstantin Mikityuk who accepted to serve as my supervisor, and went on to perform that task admirably. Additional thanks to Jiří Křepel for originally proposing the project, to Valentyn Bykov for patiently performing MCNP calculations for me, and to everyone else at PSI and in Wettingen for assistance, discussions, laughs, and kindness.

This thesis has benefited tremendously from the tireless assistance of Matteo Zanetti, whose contributions are now beyond counting. Additional insights and motivation were provided by the participants to the 3rd SAMOFAR Progress Meeting hosted in Grenoble, France.